PLOS GENETICS

RESEARCH ARTICLE

Sequencing of Argonaute-bound microRNA/mRNA hybrids reveals regulation of the unfolded protein response by microRNA-320a

Christopher J. Fields[1,2], Lu Li[1,2], Nicholas M. Hiers[1,2], Tianqi Li[1,2], Peike Sheng[1,2], Taha Huda[1], Jixiu Shan[2], Lauren Gay[2,3], Tongjun Gu[4], Jiang Bian[5], Michael S. Kilberg[1,2], Rolf Renne[2,3,6], Mingyi Xie[1,2,6]*

1 Department of Biochemistry and Molecular Biology, University of Florida, College of Medicine, Gainesville, Florida, United States of America, **2** UF Health Cancer Center, University of Florida, Gainesville, Florida, United States of America, **3** Department of Molecular Genetics and Microbiology, University of Florida, College of Medicine, Gainesville, Florida, United States of America, **4** Bioinformatics, Interdisciplinary Center for Biotechnology Research, University of Florida, Gainesville, Florida, United States of America, **5** Department of Health Outcomes and Biomedical Informatics, University of Florida, College of Medicine, Gainesville, Florida, United States of America, **6** UF Genetics Institute, University of Florida, Gainesville, Florida, United States of America

* mingyi.xie@ufl.edu

Citation: Fields CJ, Li L, Hiers NM, Li T, Sheng P, Huda T, et al. (2021) Sequencing of Argonaute-bound microRNA/mRNA hybrids reveals regulation of the unfolded protein response by microRNA-320a. PLoS Genet 17(12): e1009934. https://doi.org/10.1371/journal.pgen.1009934

Editor: Aleksandra Filipovska, The University of Western Australia, AUSTRALIA

Received: May 25, 2021

Accepted: November 8, 2021

Published: December 16, 2021

Data Availability Statement: Data generated in this publication have been deposited to the NCBI Gene Expression Omnibus (GEO) and can be accessed at GSE164634.

Funding: This work is supported by the National Institutes of Health (nih.gov) [R35-GM128753 and R00-CA190886 to M.X., R01-CA246418 and UL1-TR001427 to J.B., R01-CA203565 and R21-HD100576 to M.S.K., P01-CA214091 to R.R., T32CA257923 to N.M.H. and NIDCR T90-DE021990 to L.A.G.]; UF Health Cancer Center

Abstract

MicroRNAs (miRNA) are short non-coding RNAs widely implicated in gene regulation. Most metazoan miRNAs utilize the RNase III enzymes Drosha and Dicer for biogenesis. One notable exception is the RNA polymerase II transcription start sites (TSS) miRNAs whose biogenesis does not require Drosha. The functional importance of the TSS-miRNA biogenesis is uncertain. To better understand the function of TSS-miRNAs, we applied a modified Crosslinking, Ligation, and Sequencing of Hybrids on Argonaute (AGO-qCLASH) to identify the targets for TSS-miRNAs in HCT116 colorectal cancer cells with or without *DROSHA* knockout. We observed that miR-320a hybrids dominate in TSS-miRNA hybrids identified by AGO-qCLASH. Targets for miR-320a are enriched for the eIF2 signaling pathway, a downstream component of the unfolded protein response. Consistently, in miR-320a mimic- and antagomir- transfected cells, differentially expressed gene products are associated with eIF2 signaling. Within the AGO-qCLASH data, we identified the endoplasmic reticulum (ER) chaperone calnexin as a direct miR-320a down-regulated target, thus connecting miR-320a to the unfolded protein response. During ER stress, but not amino acid deprivation, miR-320a up-regulates ATF4, a critical transcription factor for resolving ER stress. In summary, our study investigates the targetome of the TSS-miRNAs in colorectal cancer cells and establishes miR-320a as a regulator of unfolded protein response.

Author summary

MicroRNA biogenesis factors, such as Drosha and Dicer, are frequently dysregulated in cancer, resulting in the disruption of miRNA-mediated gene regulation. Independent of

[CTHR Pilot grant to M. X. and J.B.]. The funders had no role in study design, data collection and analysis, decision to publish, or preparation of the manuscript.

Competing interests: no authors have competing interests.

Drosha-processing, transcription start site microRNA levels are elevated compared to most microRNAs in cancer cells with low *DROSHA* expression. By sequencing Argonaute-bound miRNA/mRNA pairs in colorectal cancer cells in the absence of Drosha, we identify the targetome for transcription start site microRNAs. We discovered a transcription start site miRNA, miR-320a, that down-regulates expression of the endoplasmic reticulum chaperone calnexin, activates expression of ATF4, and thus activates the unfolded protein response.

Introduction

MicroRNAs (miRNAs) are ~18–22 nucleotide non-coding RNAs that target the majority of messenger RNAs (mRNAs) for post-transcriptional regulation in a tissue-specific manner [1]. Biogenesis of miRNAs begins in the nucleus, where primary miRNA (pri-miRNA) is transcribed and folded into a stem-loop hairpin that is subsequently recognized by the Microprocessor [2,3]. The Microprocessor complex comprises two RNA-binding proteins (DGCR8) and one RNase III enzyme (Drosha) [4]. Following Drosha cleavage, Exportin-5 shuttles the resulting precursor miRNA (pre-miRNA) into the cytoplasm, where Dicer removes the loop to form a ~22 base pairs double-stranded RNA [5]. Mature miRNA is loaded onto the effector protein Argonaute (AGO), forming the RNA-induced silencing complex (RISC) [5,6]. One strand is retained as part of the RISC and guides the complex to target mRNAs. Canonically, miRNAs target mRNA's 3′ untranslated region (UTR) using their seed sequence (nucleotides 2–8) by Watson-Crick base-pairing [7]. The binding of the RISC complex leads to the recruitment of the CCR4-NOT deadenylase and DCP1-DCP2 decapping complexes for mRNA degradation [8].

While the mechanisms of canonical miRNA biogenesis are well described, the existence and importance of Dicer- or Drosha-independent modes of processing are increasingly appreciated [9,10]. One such pathway is the Dicer-independent processing of miR-451, in which AGO2 directly slices the precursor hairpin of miR-451 following its export from the cytoplasm [11–13]. While the majority of the miRNAs are increasingly down-regulated during erythrocyte differentiation, the Dicer-independent miR-451 is up-regulated [14,15]. Likewise, two distinct pathways that bypass Drosha have been identified. The mirtron pathway generates pre-miRNAs from intron splicing and then converges into the canonical pathway using nuclear-cytoplasmic transport by Exportin-5 [16–18]. The transcription start sites (TSS)-miRNA pathway directly generates pre-miRNAs at RNA polymerase II transcription start sites, negating the need for Drosha processing [19–21]. Consequently, this processing results in the pre-miRNA with a 7-methylguanosine (m^7G) cap on the 5′ end instead of the canonical 5′ monophosphate [19]. Moreover, some TSS-miRNA precursors contain extensions in their 5′ ends [21]. These TSS-miRNAs could have unique functions in development and disease, especially where the Microprocessor activity is perturbed [22].

Previously, we observed that TSS-miRNAs are enriched in HCT116 *DROSHA* knockout (KO) cells compared to wild-type (WT) cells, likely due to better access to the limited miRNA machinery (Fig 1A) [21,23]. Because TSS-miRNAs are synthesized independently of the Microprocessor, it is conceivable that they persist in diseased cell types where *DROSHA*'s function is impaired. The loss of *DROSHA* has been documented in both endometrial cancer and breast cancer [24,25]. In melanoma, Drosha levels in the nucleus are reduced, likely due to impaired cytoplasmic-nuclear import [26]. Multiple components of the miRNA biogenesis pathway are mutated in pediatric Wilms tumors, including *DROSHA*, which is down-

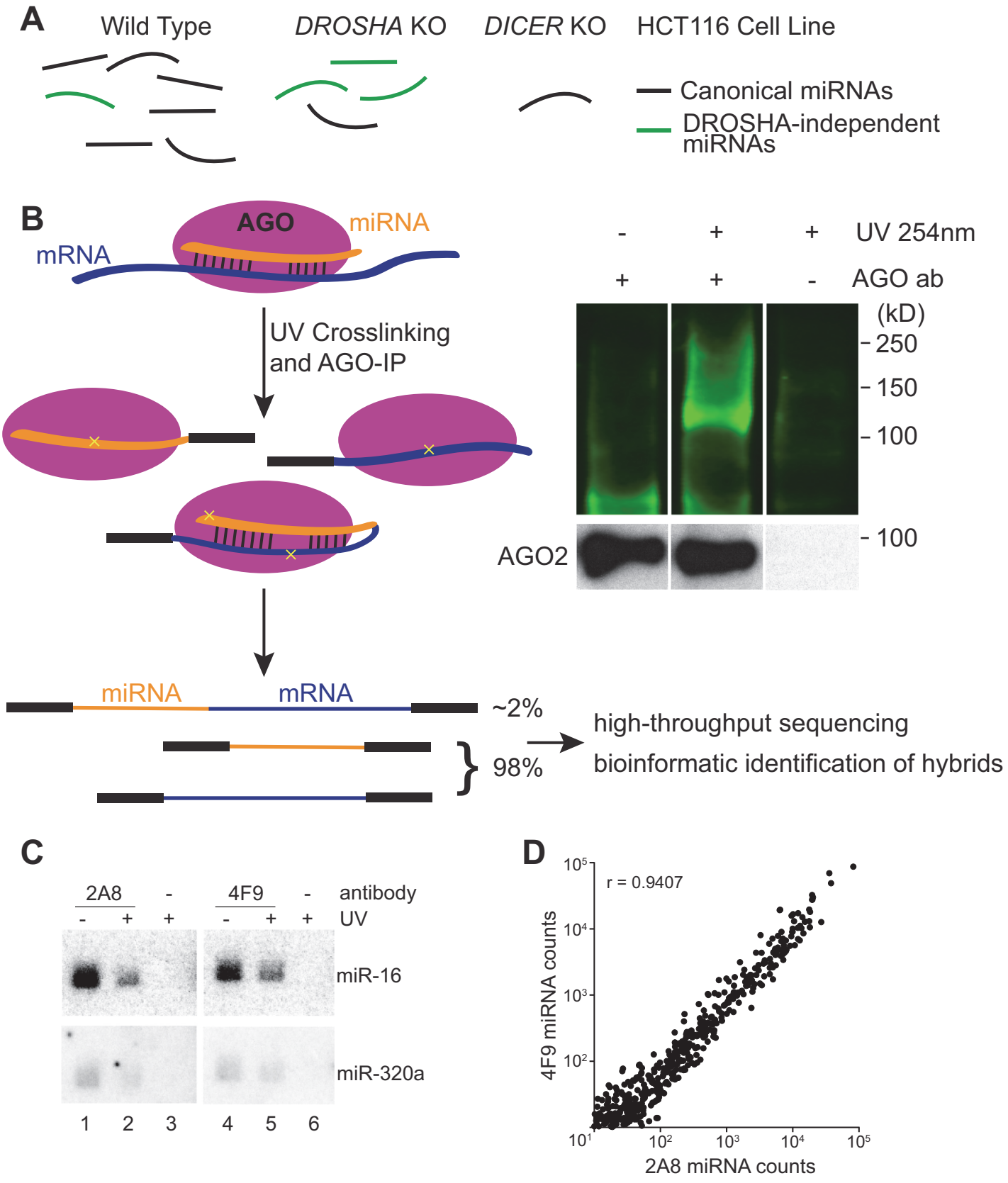
A
Wild Type
DROSHA KO
DICER KO
HCT116 Cell Line
Canonical miRNAs
DROSHA-independent miRNAs
B
AGO
miRNA
mRNA
UV Crosslinking and AGO-IP
- + + UV 254nm
+ + - AGO ab
(kD)
250
150
100
AGO2
100
miRNA
mRNA
~2%
98%
high-throughput sequencing
bioinformatic identification of hybrids
C
2A8
4F9
antibody
UV
miR-16
miR-320a
1 2 3 4 5 6
D
r = 0.9407
4F9 miRNA counts
2A8 miRNA counts

Fig 1. Argonaute crosslinking, ligation, and sequencing of hybrids in colorectal cancer cells. (A) HCT116 cell lines containing knockouts for core miRNA processing machinery allow the enrichment of Drosha-independent miRNAs (e.g., mirtrons, TSS-miRNAs). (B) Schematic of AGO-CLASH. In both CLASH and qCLASH, endogenous miRNA and mRNA are crosslinked (yellow crosses) and immunoprecipitated using AGO antibody. Following AGO-IP, the miRNA is ligated directly to its targets to form a single hybrid molecule. Each library produces hybrid reads in addition to individual reads. AGO-bound ribonucleic molecules were ligated with RA3 primer containing an IRDye 800CW, separated on a NuPAGE Bis-Tris gel, and transferred to nitrocellulose. Blots show AGO-RNA complexes detected on nitrocellulose membrane. (C) ^{32}P Northern blot of AGO-bound RNAs in HCT116 cells probed for miR-16 and miR-320a. (D) Non-hybrid miRNA reads from qCLASH libraries were quantitated with miR-Deep2. Normalized counts from qCLASH libraries that used the same AGO antibody were averaged, showing that both 2A8 and 4F9 pull down similar amounts of each miRNA. The correlation coefficient (r) is depicted on the graph.

https://doi.org/10.1371/journal.pgen.1009934.g001

regulated in around 12% of cases [27–29]. Accordingly, in the Wilms tumor cases with lower *DROSHA* expression, TSS-miRNAs, including miR-320a, miR-484, and mirtron miR-877 are up-regulated [27,30]. The consequences of *DROSHA* down-regulation and the corresponding up-regulation of TSS-miRNAs are poorly understood due to the complexity and incompleteness of the TSS-miRNA targetome.

Transcriptome-wide miRNA binding sites can be experimentally identified by crosslinking and immunoprecipitation of AGO in tandem with high throughput sequencing (e.g., HiT-S-CLIP, PAR-CLIP) [31,32]. Compared with pure bioinformatic prediction algorithms, AGO-CLIP offers the advantage of defining the miRNA targetome in cell-specific contexts. Still, AGO-CLIP protocols are laborious and require bioinformatic prediction of miRNA/target pairing, resulting in a large percentage of target sites that do not confer effective repression when bound by miRNAs [33]. Others have improved upon AGO-CLIP by directly ligating miRNAs to targets while they are base-pairing inside AGO. Such crosslinking, ligation, and sequencing of hybrids (AGO-CLASH, referred to as CLASH hereafter for simplicity) physically connects miRNA and target mRNA, allowing for high-confidence identification of the miRNA targetome [34,35]. Further iterations of CLASH, termed quick CLASH (qCLASH), have taken advantage of recent advances in bioinformatic approaches and the unprecedented depth offered by high-throughput sequencing technology. By omitting SDS-PAGE separation and purification of the protein-bound RNAs from nitrocellulose membrane, the qCLASH protocol is easier to adapt for both research and clinical purposes [36,37].

Here, we identify the targets for TSS-miRNAs using qCLASH in colorectal cancer HCT116 cells with or without Drosha. We discovered miR-320a to be the most abundant TSS-miRNA in HCT116 cells and verified that it represses targets identified by qCLASH. Pathway analysis revealed that miR-320a affects the integrated stress response (ISR), one of three pathways that collectively make up the endoplasmic reticulum (ER) unfolded protein response (UPR). Specifically, qCLASH identified the ER chaperone calnexin (CANX) as a top miR-320a target in WT and *DROSHA* KO cells. Both *CANX* mRNA and protein abundance are repressed by miR-320a. The targeting of *CANX* by miR-320a activates the ISR, a process that plays an essential role in maintaining homeostasis in the ER. Furthermore, we demonstrated that miR-320a directly targets the qCLASH-identified binding sites in the 3′ UTR of *CANX*. Consistent with previous reports, we establish that miR-320a is repressed in colorectal cancer while *CANX* is up-regulated. Investigating the downstream consequences of miR-320a perturbation of the ISR, we discovered that miR-320a can enhance *ATF4* expression in cells during ER stress. In summary, we used qCLASH to identify the targetome of miR-320a in colorectal cancer cells and established that miR-320a regulates the ISR by targeting *CANX*.

Results

CLASH for miRNA target identification in HCT116 cells

We used CLASH and its variant qCLASH to elucidate the miRNA targetomes in HCT116 cells, including WT, *DROSHA* KO, and *DICER* KO cells (Fig 1A and 1B). *DROSHA* KO cells

have elevated expression of Drosha-independent miRNAs, including TSS-miRNAs [21,38]. miRNA expression in *DICER* KO cells is abated and can serve as a background control. To minimize potential antibody specific bias, we used two different pan-AGO antibodies that can immunoprecipitate all four human AGO proteins (AGO1-AGO4) for CLASH and qCLASH. AGO antibody clone 2A8 has been widely used in the field for AGO-CLIP experiments, while clone 4F9 was less well characterized, but is locally available through the Interdisciplinary Center for Biotechnology Research at the University of Florida [31,39–42]. We found that clone 4F9 could immunoprecipitate AGO2 as effectively as the clone 2A8 (S1A Fig, lanes 3 and 7). Next, we examined AGO-associated miRNAs that are enriched by the two different antibodies. Northern blot analyses showed that canonical miRNA (miR-16) and TSS-miRNA (miR-320a) could be efficiently isolated from cells with or without 254 nm ultraviolet (UV light) crosslinking using either antibody (Fig 1C). Furthermore, high-throughput sequencing experiments revealed that miRNAs co-precipitated with AGO by both antibodies are highly correlated (Fig 1D; r = 0.9407). Therefore, we concluded that the efficacy of the 4F9 antibody rivals the widely used 2A8 antibody, and thus both are suitable for CLASH experiments.

Following immunoprecipitation, AGO-bound RNAs were digested with RNase A, modified at the termini by T4 polynucleotide kinase, and finally intermolecularly ligated together with RNA ligase, forming a single hybrid molecule (see Materials and Methods for details). For both the CLASH and qCLASH protocols, we ligated a custom pre-adenylated 3′ adapter (S1 Table). Compared to qCLASH, the CLASH protocol includes SDS-PAGE to separate crosslinked AGO-RNA complexes, which are then transferred to a nitrocellulose membrane and excised according to the appropriate molecular weight (Figs 1B and S1B). For both CLASH and qCLASH protocols, RNAs were purified from protein complexes, ligated with 5′ adapter, reverse transcribed, and PCR amplified to be compatible with Illumina sequencing (S1C Fig).

Paired-end sequencing reads obtained from qCLASH were filtered using Trimmomatic to remove low-quality reads and adapter sequences [43]. Forward and reverse reads were combined using Pear to form a single sequence for analysis [44]. Because the 5′ and 3′ adapters contain degenerate nucleotides to account for PCR bias and minimize ligation preferences [45], we collapsed duplicate reads using the FASTX-Toolkit FASTQ Collapser, and the degenerate nucleotides were removed using Cutadapt [46,47]. Chimeric reads (hybrids) were identified using the Hyb software with the default database supplemented with previously identified TSS-miRNAs and miR-snaR [21,48,49]. With viennad-format files output from Hyb, we used a custom script to identify overlapping targets for specific miRNAs. CLASH libraries were analyzed as described above, except that FASTX-Toolkit FASTQ Collapser and Cutadapt were not used since the adapters used for these libraries do not contain random nucleotides.

Comparison of CLASH, qCLASH, and miRNA-specific qCLASH

We initially performed a single biological replicate of CLASH and qCLASH using 2A8 AGO antibody in each HCT116 cell line (WT, *DROSHA* KO, and *DICER* KO). For CLASH, two regions that correspond to a molecular weight of 110–125 kD and 125–150 kD, which contain AGO crosslinked with different lengths of RNAs, were excised from the membrane (S1B Fig). As expected, in data sets obtained from *DROSHA* KO cells, we observed enrichment of hybrids containing Drosha-independent miRNAs including TSS-miRNAs (miR-320a and miR-484), mirtron (miR-877), and the recently described miR-snaR, a non-canonical miRNA derived from non-coding RNA snaR-A (S2 Table) [49]. MiR-320a-containing hybrids are far more abundant than other Drosha-independent miRNAs, comprising up to 74.58% of all the miRNA/mRNA hybrids in qCLASH data (S2 Table). Overall, with comparable amounts of raw reads obtained from both WT and *DROSHA* KO cells, we identified approximately four times

more miRNA/mRNA hybrids in qCLASH compared with CLASH (70,124: 16,487 for WT, and 4,752: 1,558 for *DROSHA* KO) (S2 Table). For miR-320a specifically, qCLASH hybrids are six to eight times more abundant than CLASH hybrids (4,511: 543 for WT, and 3,544: 597 for *DROSHA* KO) (S2 Table). Notably, approximately 50% of the CLASH hybrids can be found in qCLASH hybrids (Fig 2A and 2B). The results document that more miRNA targeting interactions were detected by qCLASH compared to CLASH.

Aside from dominant miR-320a hybrids, we found limited numbers of hybrids for other Drosha-independent miRNAs. A possible remedy to identify more targets for less abundant miRNAs would be to use a miRNA specific primer to generate a qCLASH library (S2A Fig) (see Materials and Methods for details) [50]. As a proof-of-concept experiment, we performed miR-320a-qCLASH using the same cDNA generated from qCLASH. From approximately 1/10 of the raw reads compared with qCLASH, we identified 1,271 miR-320a/mRNA hybrids, a third of which were identified by qCLASH (S2 Table). Over half of the miR-320a-qCLASH targets overlapped with the qCLASH targets (S2B Fig), suggesting that miR-qCLASH is a possible alternative to detect miRNA-specific hybrids. However, given the abundance of miR-320a in HCT116 cells, it is likely to be the only TSS-miRNA having an impactful regulation on gene expression [7]. Because of the far greater number of hybrids identified by qCLASH and the high degree of overlap with CLASH and miR-qCLASH hybrids, we opted to perform additional qCLASH replicates moving forward.

Qualitative analyses of qCLASH data sets

We generated four additional libraries for WT cells and three each for *DROSHA* KO and *DICER* KO cells. Consistent with the first qCLASH biological replicate, TSS-miRNA-containing hybrids were enriched in *DROSHA* KO cells but depleted in *DICER* KO cells (Tables 1 and S2). Comparing the miRNA counts in WT and *DROSHA* KO cells, we found that Drosha-independent miRNAs were elevated in the *DROSHA* KO cells while canonical miRNAs were repressed (Figs 2C, S3A, and S3B). We were able to identify 23,723 miR-320a/mRNA hybrids between the WT and *DROSHA* KO cells, making up 5.23% and 65.05% of the WT and *DROSHA* KO miRNA/mRNA hybrid reads, respectively. Somewhat surprisingly, even though the miR-320a counts are elevated in *DROSHA* KO compared with WT qCLASH, numbers of miR-320a/mRNA hybrids in both qCLASH data sets are comparable. This is most likely due to consistently lower levels of AGO immunoprecipitated from UV-crosslinked *DROSHA* KO cells for unknown reasons (S1B Fig, western blot). Amongst all the Drosha-independent miRNAs, miR-320a hybrids were the most abundant, reflecting miR-320a's dominance in HCT116 cells. Few hybrids were identified for other TSS-miRNAs (S3 Table). In conclusion, we used *DROSHA* KO cells to enrich Drosha-independent miRNAs and identified prevailing miR-320a hybrids in qCLASH.

Previous CLASH studies reported that miRNA abundance correlates with the number of hybrids of each miRNA [35]. Averaging five WT qCLASH data sets, we found a strong correlation between miRNA abundance and the number of hybrids identified for each miRNA (Fig 2D; r = 0.7877). In contrast, we found no positive correlation between transcript abundance and hybrid count (S3C Fig; r = -0.04855,). Therefore, targets enriched in miR-320a hybrids are not due to their transcript abundance, but because of their specific interaction with miR-320a.

We next analyzed the binding location of miRNAs using the qCLASH data and found that miRNAs primarily target the CDS and 3′ UTR as previously reported (Fig 2E) [31,34–37]. Canonical miRNA interactions involve the miRNA seed region, usually nucleotides 2–7 and sometimes nucleotide 8 on the miRNA [7]. However, previous CLASH studies have demonstrated substantial non-seed targeting [34–36]. Similarly, we found that non-seed binding,

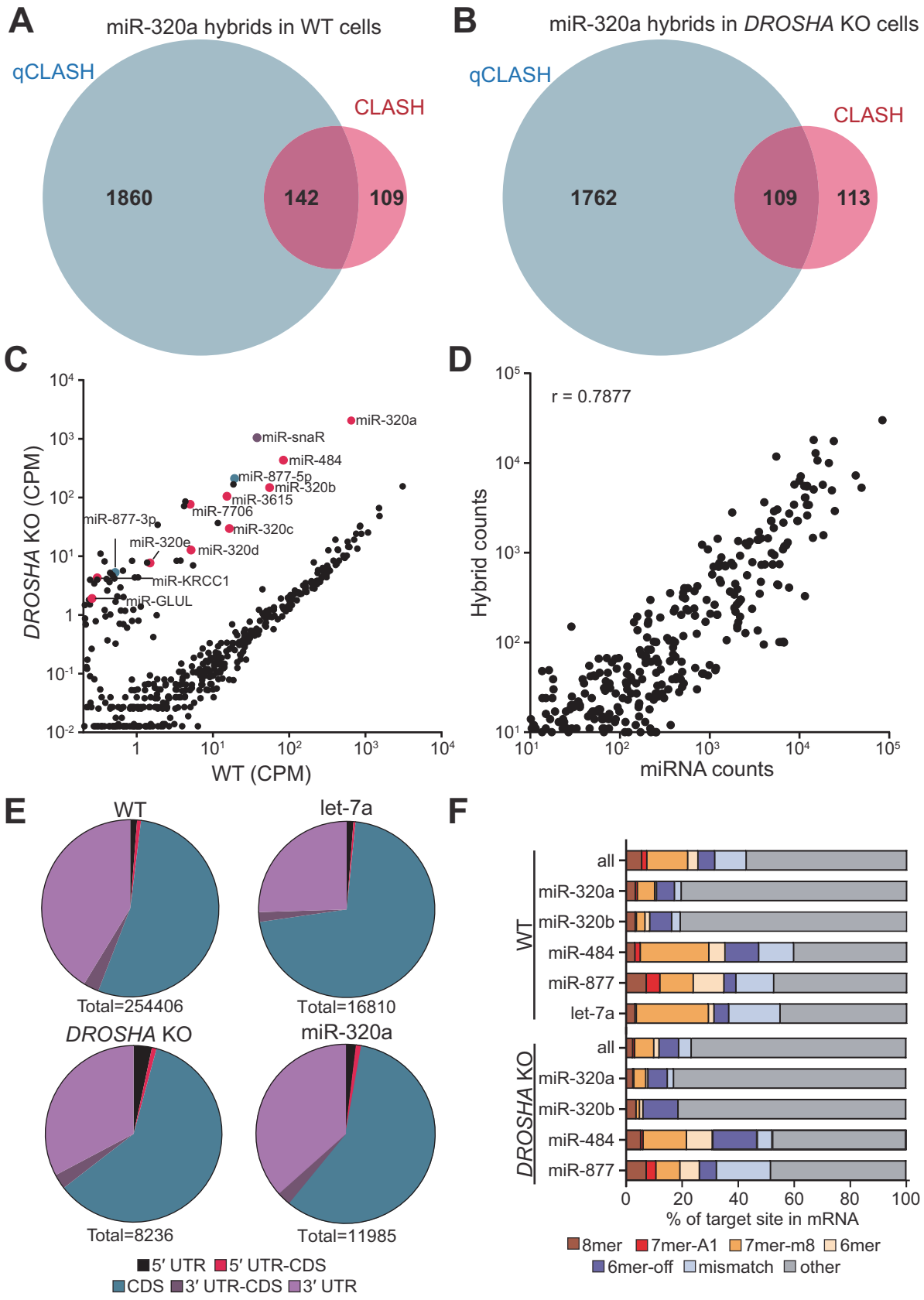
A
miR-320a hybrids in WT cells
qCLASH
CLASH
1860
142
109
B
miR-320a hybrids in DROSHA KO cells
qCLASH
CLASH
1762
109
113
C
DROSHA KO (CPM)
WT (CPM)
miR-320a
miR-snaR
miR-484
miR-877-5p
miR-320b
miR-3615
miR-7706
miR-320c
miR-877-3p
miR-320e
miR-320d
miR-KRCC1
miR-GLUL
D
r = 0.7877
Hybrid counts
miRNA counts
E
WT
let-7a
Total=254406
Total=16810
DROSHA KO
miR-320a
Total=8236
Total=11985
5′ UTR
5′ UTR-CDS
CDS
3′ UTR-CDS
3′ UTR
F
WT
DROSHA KO
all
miR-320a
miR-320b
miR-484
miR-877
let-7a
% of target site in mRNA
8mer
7mer-A1
7mer-m8
6mer
6mer-off
mismatch
other

Fig 2. Analysis of AGO-qCLASH in HCT116 colorectal cancer cells. Venn diagram depicting the overlap of miR-320a target genes in qCLASH and CLASH for (A) WT cells and (B) *DROSHA* KO cells. (C) Normalized read count of miRNAs in HCT116 and HCT116 *DROSHA* KO cells. miRNA counts were determined with miR-Deep2 and normalized to total reads. TSS-miRNAs are labeled in magenta, mirtrons are labeled in green, miR-snaR is labeled in purple, and all other miRNAs are labeled in black. (D) Correlation plot of miRNA abundance and hybrid counts for each miRNA. miRNA counts were determined using miR-Deep2 and normalized to total number of reads. The number of hybrids for each miRNA was determined and plotted against miRNA counts. A correlation coefficient (r) is provided. (E) miRNA target sites are found predominately in the CDS and 3′UTR. The location of each transcript from the mRNA portion of the hybrid was determined using data from Ensemble Biomart. Each hybrid was assigned a location based on where it was located in relation to the beginning and end of the reference CDS. Transcripts with IDs not found in the database were excluded from the analysis. (F) The proportion of hybrids with seed binding was less than non-canonical pairings. Seed binding was determined using viennad files, which predicts folding between the miRNA and its target. Individual miRNAs display distinct distributions of seed bindings.

https://doi.org/10.1371/journal.pgen.1009934.g002

including mismatches, makes up most of the miRNA-target interactions in WT cells (Fig 2F). Interestingly, we found that miR-320a has more non-seed matches than other miRNAs examined. Given miR-320a's abundance in *DROSHA* KO cells, it is not surprising that the total miRNA-interactions in *DROSHA* KO closely matches miR-320a's interactions (Fig 2E and 2F). Taken together, qualitative analyses of the qCLASH data are consistent with previous reports, suggesting that we successfully captured endogenous miRNA/mRNA interactions [34].

Identification of miR-320a targets with qCLASH

While *DROSHA* KO cells were enriched in Drosha-independent miRNAs including TSS-miRNAs, only miR-320a hybrids were abundant enough to facilitate robust analysis of its functions. To understand the function of miR-320a, we interrogated qCLASH identified targets in at least two replicates in WT or *DROSHA* KO cells with Ingenuity Pathway Analysis (IPA) to identify cellular pathways regulated by miR-320a (S4 and S5 Tables). eIF2 signaling was identified as the most enriched pathway in WT qCLASH (Figs 3A and S4A). The top ten most significantly enriched pathways for miR-320a targets in WT qCLASH are also significantly enriched in *DROSHA* KO qCLASH (Fig 3A).

Table 1. Summary of AGO-qCLASH in HCT116 cells. The table depicts the total number of miRNA/mRNA reads in each qCLASH sample. miR-320a/mRNA reads are broken down by replicate and summed for each sample group. Percentage depicts the fraction of miR-320a hybrids in total miRNA/mRNA hybrids. BR = Biological replicate.

	HCT116 Cell Line	AGO Antibody	miRNA/mRNA Hybrids	miR-320a/mRNA Hybrids	
qCLASH	**Wild Type**		**303,980**	**15,902**	**5.23%**
	BR1	2A8	70,124	4,511	6.43%
	BR2	4F9	64,561	3,695	5.72%
	BR3	2A8	32,940	1,942	5.90%
	BR4	2A8	59,250	2,399	4.05%
	BR5	4F9	77,105	3,355	4.35%
	DROSHA KO		**12,023**	**7,821**	**65.05%**
	BR1	2A8	4,752	3,544	74.58%
	BR2	2A8	1,739	1,171	67.34%
	BR3	4F9	2,562	1,481	57.81%
	BR4	4F9	2,970	1,625	54.71%
	DICER KO		**3,044**	**108**	**3.55%**
	BR1	2A8	662	22	3.32%
	BR2	2A8	1,005	42	4.18%
	BR3	4F9	886	31	3.50%
	BR4	4F9	491	13	2.65%

https://doi.org/10.1371/journal.pgen.1009934.t001

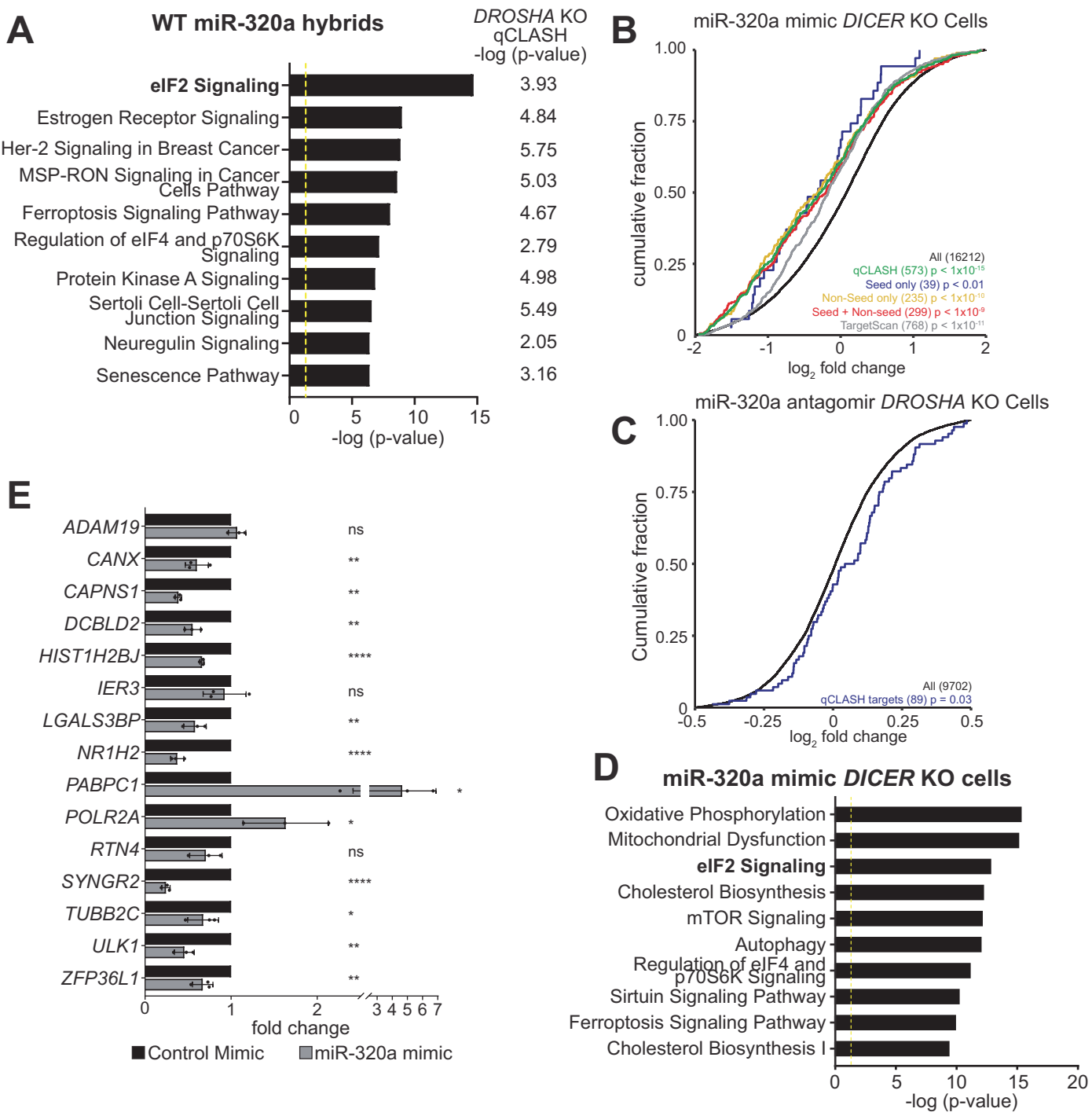

Fig 3. Identification of pathways targeted by miR-320a in HCT116 cells. (A) Top ten pathways targeted by miR-320a in WT qCLASH. The corresponding -log (p-value) for each pathway in *DROSHA* KO qCLASH is depicted right of each bar. The yellow line defines significance threshold for IPA. (B) The cumulative distribution function of fold change in gene expression for qCLASH-identified miR-320a targets (in $\geq$ 3 WT replicates) following miR-320a mimic transfection in HCT116 *DICER* KO cells. Green line: all qCLASH identified targets; Blue line: qCLASH-identified targets containing only seed matches; Yellow line: qCLASH-identified targets containing only non-seed matches; Red line: miR-qCLASH-identified targets that contain both seed and non-seed matches; Gray line: conserved miR-320a targets predicted by TargetScan; Black line: all transcripts. P-values were determined using Kolmogorov Smirnov tests between colored subsets and control (black). (C) The cumulative distribution function of fold change in gene expression for qCLASH-identified miR-320a targets (in $\geq$ 4 WT replicates, blue line) following miR-320a antagomir transfection in HCT116 *DROSHA* KO cells. (D) Top 10 pathways enriched in differentially expressed genes ($p \leq 0.05$) from (B) were determined by IPA. (E) High-confidence targets from qCLASH were validated using RT-qPCR. HCT116 *DICER* KO cells were transfected with miR-320a mimic or non-specific control. Total RNA was prepared and gene expression was measured with RT-qPCR using the comparative Ct method and depicted as fold changes. Data are shown as the average of three biological replicates with a standard deviation. ns = $P > 0.05$, * = $P \leq 0.05$, ** = $P \leq 0.01$, **** = $P \leq 0.0001$.

https://doi.org/10.1371/journal.pgen.1009934.g003

Previously, others have demonstrated that predicted miRNA targetomes can be evaluated by measuring the transcriptome-wide gene expression change following exogenous expression of miRNAs [51,52]. miRNA mimics are exogenously expressed RNAs that function the same as miRNAs while antagomirs block the function of miRNAs. Therefore, we used miRNA mimic or antagomir transfection coupled with RNA-sequencing to validate the large number of miR-320a targets identified in qCLASH. It has been noted that transfection of excess miRNA mimics could perturb normal miRNA function via competition with the endogenous miRNAs [23,53]. Since gene expression in *DICER* KO cells is under minimal regulation by endogenous miRNAs, we transfected miR-320a mimic in both WT and *DICER* KO cells and measured global gene expression change using RNA-sequencing. Conversely, antagomir was transfected into *DROSHA* KO cells, which exhibit high endogenous miR-320a expression, to inhibit miR-320a [21]. As a validation of the functionality of miR-320a mimic and antagomir, we also transfected WT, *DROSHA* KO and *DICER* KO cells expressing a GFP reporter with two complementary miR-320a binding sites (S5A Fig–upper left panel) [21]. In mimic-transfected WT and *DICER* KO cells, a reduction of GFP was observed, signifying that the mimic was loaded onto the RISC complex and was functional (S5A Fig). In contrast, an increase in GFP was observed in miR-320a antagomir-transfected *DROSHA* KO cells. On northern blots, the mimic drastically increased miR-320a levels in WT and *DICER* KO cells, while an almost complete inhibition of miR-320a was detected in *DROSHA* KO cells transfected with the antagomir (S5B Fig) [54,55]. These results confirm the efficacy of the miR-320a mimic and antagomir in HCT116 cells.

Consistent with miRNA's repressive function in mRNA abundance, in RNA-seq of miR-320a-transfected *DICER* KO cells, we found significant repression of qCLASH-identified targets that appear in at least three WT qCLASH replicates (Fig 3B, green curve, $p < 1.0x10^{-5}$). The degree of repression for qCLASH-identified targets is greater when compared with TargetScan-predicted targets (Fig 3B, $p < 10^{-11}$, compare green curve with the gray curve). Given that qCLASH detected a large portion of non-seed targets for miR-320a (Fig 2F), we examine whether these non-seed targets react differently to miR-320a mimic transfection compared to the canonical seed-match targets. To this end, qCLASH-identified miR-320a targets were classified into three different groups for analysis: targets with only seed match sites (blue curve); targets with only non-seed binding sites (yellow curve), and targets with both seed and non-seed binding sites (red curve). Targets in different groups were repressed by miR-320a mimic to similar extents, suggesting that both seed and non-seed sites are functional (Fig 3B).

To confirm that miR-320a represses its targets at the physiological level, we analyzed fold changes of miR-320a targets in *DROSHA* KO cells transfected with miR-320a antagomir. miR-320a targets identified in at least three WT qCLASH replicates trended toward derepression, although the change was not statistically significant (S5C Fig, red curve, $p = 0.09$). Similarly, TargetScan-predicted targets did not show derepression compared with all transcripts (S5C Fig, cyan curve, $p = 0.14$). We reasoned that the lack of significant derepression is because blocking miRNA induces more subtle changes in target expression compared with mimic transfection. Therefore, we further extracted high-confidence miR-320a targets identified in 4 out of 5 WT qCLASH replicates. These targets were indeed significantly derepressed when miR-320a was inhibited by antagomir (Fig 3C, $p = 0.03$), confirming that qCLASH-identified targets are regulated by miR-320 in physiological conditions.

By IPA, the differentially expressed mRNAs in *DICER* KO cells transfected with miR-320a were further analyzed and the eIF2 signaling pathway was once again one of the most significantly enriched pathways (Figs 3D and S4B, $p \leq 0.05$), consistent with the observation that this pathway was enriched in qCLASH-identified targets (Figs 3A and S4A). Consistently, transcriptomic analyses of miR-320a mimic-transfected WT cells and antagomir-transfected

DROSHA KO cells show that the eIF2 signaling pathway ranked near the top of the list of most significantly altered pathways determined by IPA (S6 Fig).

To validate individual qCLASH targets, we performed real-time quantitative PCR following reverse transcription (RT-qPCR) on total RNAs extracted from miR-320a-transfected *DICER* KO cells. We selected individual qCLASH targets that appear in 4 of the 5 WT datasets, as well as in 3 out of 4 *DROSHA* KO datasets, generating a list of 15 high-confidence miR-320a targets (S7 Fig). The mRNA portion of each hybrid contains putative miR-320a binding sites that reside within the 3′ UTR or the CDS. Seven of the genes contain canonical miR-320a binding sites in the 3′ UTR. In RT-qPCR, ten of the targets were repressed, two were up-regulated, and three showed no significant change (Fig 3E). For the targets containing canonical seed matches, all but one were repressed. Therefore, both global RNA-seq and targeted RT-qPCR experiments confirmed that qCLASH identified genuine miR-320a targets.

miR-320a represses chaperone protein calnexin

Given that the eIF2 signaling pathway is enriched in miR-320a qCLASH targets and in differentially expressed genes when the miR-320a level changes, we reasoned that a miR-320a target affecting this pathway would be present in both WT and *DROSHA* KO qCLASH. Among the top 15 high confidence miR-320a targets, the transmembrane endoplasmic reticulum (ER) chaperone protein calnexin (CANX) directly connects with eIF2 signaling. CANX works in tandem with calreticulin (CALR) to assist in folding glycoproteins or designating unfolded proteins to the proteasome [56–58]. When unfolded proteins accumulate in the ER, the three UPR pathways, one of which is the eIF2-mediated ISR, get activated to increase *CANX*/*CALR* expression to help alleviate the stress of mis-folded proteins [59–61]. In both RNA-seq and RT-qPCR data, *CANX* mRNA was repressed in response to miR-320a mimic transfection (Figs 3E and 4A). miR-320a not only lowered *CANX* mRNA, but also reduced the quantity of CANX protein, as western blot-detected CANX protein levels are significantly repressed in WT cells treated with miR-320a mimic (Fig 4B). When miR-320a was repressed by antagomir in WT cells, up-regulation of CANX was observed (Fig 4C).

In our list of high confidence targets, *CANX* has one miR-320a target sequence in the 3′ UTR (S7 Fig). Additionally, when we examined targets that appeared in fewer qCLASH replicates, we identified an additional binding site within 100 nts of the high confidence *CANX* site. Both sites contain strong canonical seed binding (Fig 4D). We cloned the *CANX* 3′ UTR containing both qCLASH-identified binding sites downstream of the firefly luciferase within a dual-luciferase reporter. When we co-transfected the WT reporter with a plasmid that encodes miR-320a in HEK 293T cells, reduced expression of the firefly luciferase was observed (Fig 4E). Using site-directed mutagenesis, we changed both miR-320a binding sites to miR-HSUR4 sites. miR-HSUR4 is a viral miRNA that is not endogenously expressed in 293T cells. In both cases, neither site mutant alone was able to derepress the firefly reporter completely. This finding suggests that a single site is sufficient for miR-320a mediated repression of *CANX*. When both sites are mutated, the firefly luciferase signal increased, demonstrating that both sites are bona fide miR-320a binding sites (Fig 4E).

We next sought support for miR-320a targeting of *CANX* from patient data available in The Cancer Genome Atlas (TCGA) [62,63]. We found that miR-320a was most down-regulated in colorectal cancer compared to other cancer types (S8A Fig). Previous reports of miR-320a expression in colorectal cancer demonstrated lower expression when compared to non-tumor tissue [64,65]. Decreasing expression of miR-320a is associated with poor prognosis in colorectal cancer patients [66–68]. Conversely, increased *CANX* expression was associated with poor clinical outcomes in colorectal cancer patients [69]. We analyzed patient samples where both

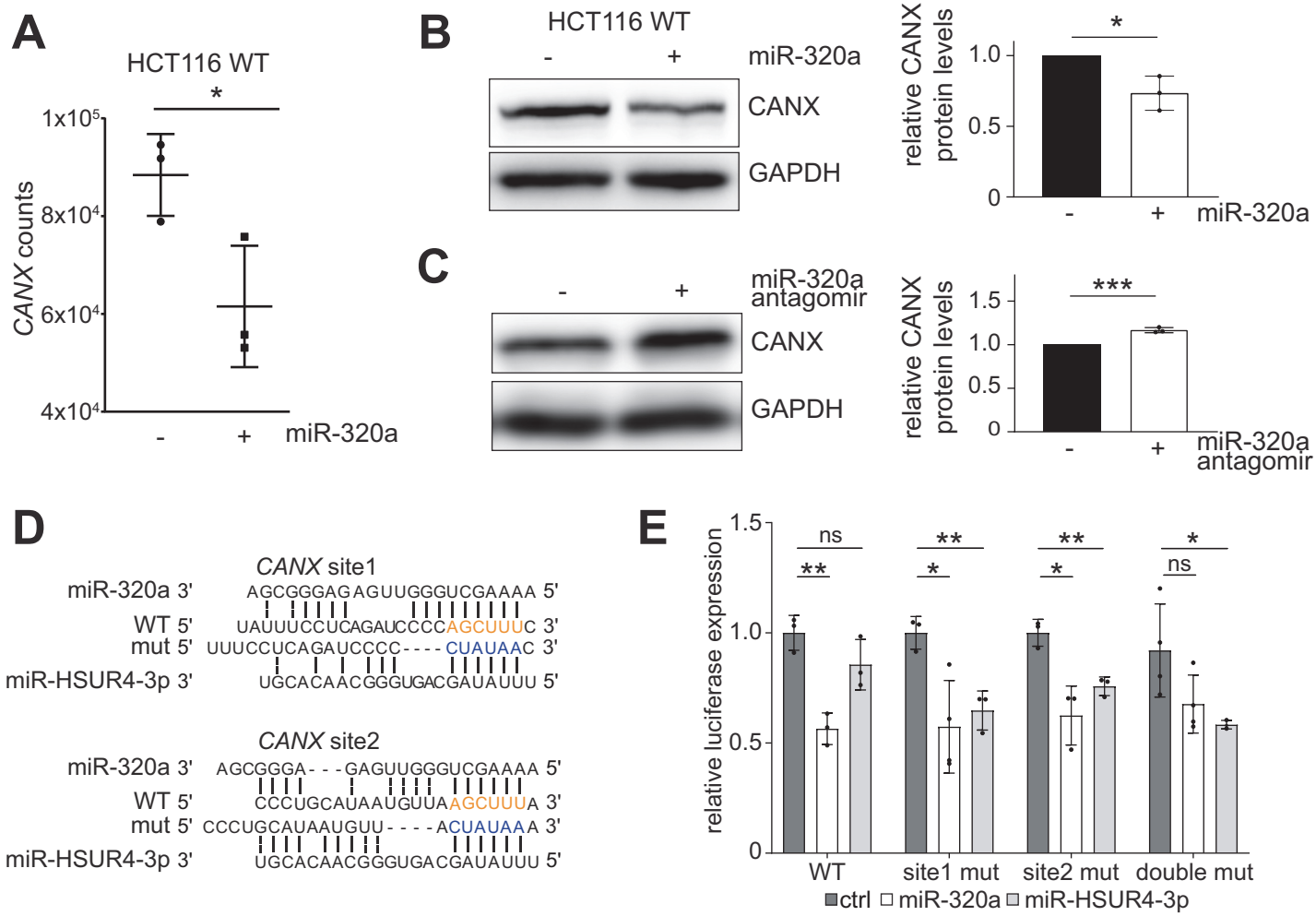

Fig 4. miR-320a targets CANX in colorectal cancer cells to activate UPR. (A) *CANX* expression is reduced in miR-320a mimic transfected *DICER* KO cells, measured by RNA-seq. Gene counts were generated from Stringtie output and normalized using Deseq2. Individual samples were plotted along with mean and standard deviation, for three biological replicates. * = $P \leq 0.05$. Western blots of CANX in miR-320a mimic (B) and antagomir (C) transfected HCT116 cells. GAPDH was used as a loading control. Quantitation of CANX protein expression is depicted in bar graphs as individual points with standard deviation for three biological replicates. * = $P \leq 0.05$, *** = $P \leq 0.001$. (D) Predicted base-pairing of miR-320a and miR-HSUR4-3p with *CANX* 3′ UTR; miR-320a seed match sequence on *CANX* is highlighted in orange; miR-HSUR4-3p seed match sequence is highlighted in blue. (E) Dual-luciferase reporter containing WT *CANX* 3′ UTR miR-320a binding sites, a mutation in site 1 (site 1 mut), a mutation in site 2 (site 2 mut), or double mutant was co-transfected with a vector expressing miR-320a, miR-HSUR4-3p, or an empty vector in 293T cells. All luciferase assays were performed in technical and biological triplicates. ns = $P > 0.05$, * = $P \leq 0.05$, ** = $P \leq 0.01$.

https://doi.org/10.1371/journal.pgen.1009934.g004

mRNA and miRNA sequencing were performed using the same tissue [70,71]. miR-320a was down-regulated in six out of the seven tumors, matching previous reports and TCGA data (S8B Fig) [66–68,72–74]. Conversely, *CANX* was up-regulated in six out of the seven of the tumors analyzed (S8C Fig). Together with our biochemical characterization of the miR-320a target sites in *CANX* mRNA, these results suggest an inverse relationship between the expression of miR-320a and *CANX*.

miR-320a activates the unfolded protein response

The accumulation of unfolded proteins in the ER results in the activation of a trio of ER-resident proteins (IRE1, PERK, and ATF6) that triggers three separate signaling pathways,

collectively known as the UPR. These three proteins create a torrent of signals directed at either reducing the stress or leading towards programmed cell death (apoptosis) [60]. We hypothesized that down-regulation of *CANX* by miR-320a would lead to the accumulation of unfolded proteins. In response to unfolded protein accumulation, IRE1 dimerizes and autophosphorylates, activating its RNase domain to cleave a 26-base unconventional intron out of *XBP1* mRNA [61]. This unique splicing allows the translation of the active form of XBP1 which in turn activates the transcription of UPR responsive genes. To determine if miR-320a affects the UPR, we measured the active (i.e., spliced) form of *XBP1* mRNA using RT-qPCR in miR-320a mimic-transfected WT cells. Primers spanning the 26 bp region spliced out by IRE1 were used to measure the amount of spliced *XBP1* [75]. We found that miR-320a increases the splicing of *XBP1* (Fig 5A), in agreement with a previous report that knockout of *CANX* induced IRE1-mediated splicing of *XBP1* and the constitutive activation of the UPR [58]. Furthermore, we measured the levels of *BiP* and *CHOP*, downstream genes activated by the UPR. *BiP* and *CHOP* mRNAs in WT cells are up-regulated by miR-320a mimic transfection, further supporting the role of miR-320a in activating UPR (Fig 5A).

Activation of the *PERK* arm of the UPR leads to a suppression of global protein synthesis, but at the same time to the translational induction of a well characterized effector, Activating Transcription Factor 4 (*ATF4*) [59]. This translational control mechanism, termed the ISR, is also observed for other cellular stress responses, including amino acid deprivation leading to the presence of uncharged tRNAs [60,76,77]. Given miR-320a's involvement in UPR via targeting *CANX*, we reasoned that miR-320a might affect *ATF4* expression under ER stress induced by unfolded proteins. To this end, we transfected miR-320a in WT HCT116 cells and treated them with either thapsigargin (Tg) or tunicamycin (Tm). Tg is an endoplasmic reticulum Ca^{2+} ATPase inhibitor that prevents the import of Ca^{2+} into the lumen of the ER [61,78]. Tm blocks protein N-glycosylation [79]. Both treatments ultimately result in the accumulation of unfolded proteins. As expected, ATF4 protein levels increased upon Tg- and Tm- treatment (Fig 5B), and cells transfected with miR-320a showed exacerbated up-regulation of *ATF4* (Fig 5B, compare lane 3 to lane 4, lane 5 to lane 6), while cells transfected with miR-320a antagomir showed lower *ATF4* up-regulation (Fig 5C, compare lane 3 to lane 4). To test whether the miR-320a up-regulated *ATF4* expression is specific to the UPR, we repeated miR-320a transfection with the addition of histidinol, an amino acid alcohol that mimics stress induced by amino acid deprivation [80]. No significant change in *ATF4* expression with or without miR-320a transfection was detected, which suggests the miR-320a-mediated change in *ATF4* is specific to the UPR (Fig 5B, compare lane 7 to lane 8).

Given that up-regulation of *ATF4* in response to stress is transient, we conducted a time-course experiment to observe *ATF4* expression in the presence of Tg-treatment and miR-320a transfection over time. As before, we found that miR-320a increases *ATF4* expression in stress-induced HCT116 and Human embryonic kidney (HEK) 293T cells, which peaked at 4 hours after Tg-treatment (S9A and S9B Fig). CANX was initially repressed, before being up-regulated towards later time points in miR-320a overexpressed cells, signifying that CANX expression is activated in response to the ATF4 up-regulation (S9A and S9B Fig). During Tg treatment, we observed that miR-320a levels remain constant in HCT116 cells, but miR-320a cannot be detected by northern blot in 293T cells (S9C and S9D Fig).

We next examined if expressing miR-320a closer to the physiological level in cells would also enhance *ATF4* up-regulation. HEK 293T cells express low levels of miR-320a and transfection of a plasmid containing miR-320a gene under the control of its native promoter enables miR-320a expression [19]. Similar to miR-320a mimic transfection in HCT116 cells, we observed up-regulation of *ATF4* in both Tg- and Tm- treated 293T cells when miR-320a was expressed from the plasmid (S10A Fig, compare lane 3 to lane 4, lane 5 to lane 6).

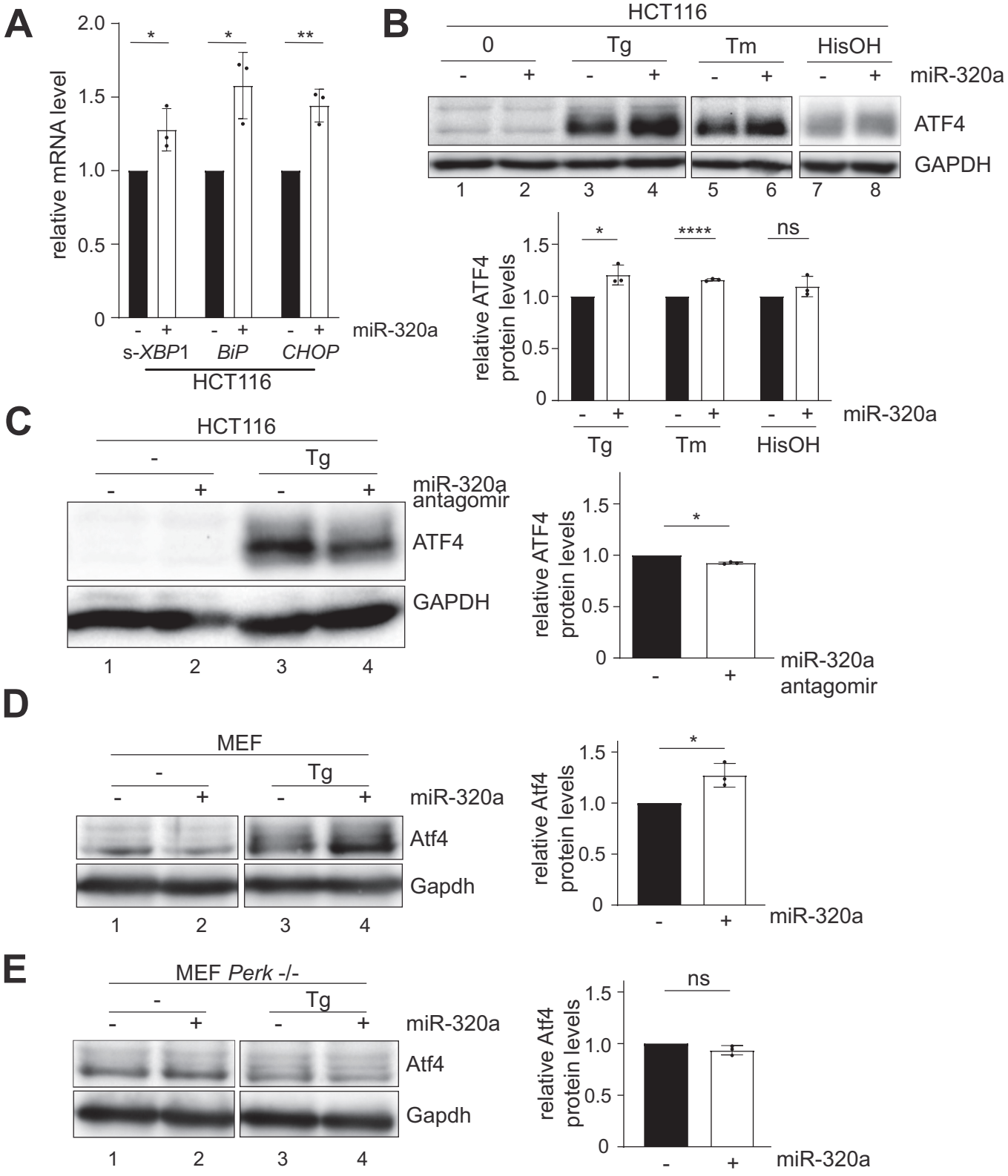

Fig 5. miR-320a activates ATF4 during ER stress. (A) RT-qPCR quantification of spliced(s)-*XBP1*, *BiP*, and *CHOP* mRNA in HCT116 cells transfected with miR-320a mimic. Data are shown as the average of three biological replicates with a standard deviation and individual data points. All three mRNAs were normalized to *HPRT*. Experiments were performed in technical triplicate. (Student's t-test): ns = $P > 0.05$, * = $P \leq 0.05$, ** = $P \leq 0.01$. (B) Western blots of ATF4 in miR-320a

mimic-transfected WT cells with thapsigargin (Tg), tunicamycin (Tm) or histidinol (HisOH) treatment. (C) Western blots of ATF4 in miR-320a antagomir-transfected HCT116 with Tg treatment. Western blots of Atf4 in miR-320a mimic-transfected MEF WT (D) and Perk -/- cells (E) with Tg treatment. In all western blots, GAPDH was used as a loading control. Quantitation of three biological replicates with mean and standard deviation is shown with individual data points. (Student's t-test): ns = $P > 0.05$, * = $P \leq 0.05$, **** = $P \leq 0.0001$.

https://doi.org/10.1371/journal.pgen.1009934.g005

Finally, we tested whether UPR regulation by miR-320a occurs in other cell lines. Upon transfecting miR-320a mimic in cells with low endogenous miR-320a, such as glioblastoma T98G cells, HeLa cells and mouse embryonic fibroblast (MEF) cells, Tg-induced *ATF4* activation was further elevated (Figs 5D, S10B and S10C, compare lane 3s to lane 4s). On the other hand, we transfected miR-320a antagomir in medulloblastoma DAOY cells, in which endogenous miR-320a levels are high and treated the cells with Tg. As expected, inhibition of miR-320a dampened the activation of *ATF4* in DAOY cells (S10D Fig, compare lane 3 to lane 4). With MEF cells, we further utilized a previously established *Perk* -/- line to test whether *Atf4* up-regulation is directly connected with UPR [81]. Accumulation of unfolded proteins in the ER causes the dissociation of the protein BiP from PERK, allowing it to dimerize. Auto-phosphorylation of PERK dimer is essential to activate the ISR response. Indeed, in MEF cells without Perk, miR-320a mimic transfection failed to trigger *Atf4* activation (Fig 5E, compare lane 3 to lane 4). In summary, miR-320a's regulation of UPR is observed in diverse cell lines.

Discussion

qCLASH allows for the identification of endogenous miRNA/target pairing

Bioinformatic predictions based on seed binding of miRNA with mRNA 3′ UTR have expanded our understanding of miRNAs' functions. However, recent studies using CLASH have identified significant miRNA binding events that do not require perfect seed base-pairing as well as miRNA binding to regions other than the 3′ UTR [34–37,82]. This study identified seven high-confidence non-canonical miR-320a targets including eleven different target sites in both the 3′ UTR and the CDS (S7B Fig). Amongst these genes, four were repressed, two were up-regulated, and one was not significantly affected (Fig 3E). Likewise, other studies have documented non-canonical pairings. For example, miR-20a exclusively targets *DAPK3* in the CDS region, but not when the site is moved to the 3′ UTR of a luciferase reporter [83]. Additionally, miR-20a targeting of *DAPK3* represses gene expression by blocking translation instead of targeting the mRNA for decay. In addition to novel binding sites, several studies have documented the presence and efficacy of non-seed matches, including uridylated miR-124 having a distinct targetome from canonical miR-124 [50,51,84]. Among the high confidence miR-320a targets we identified here, seed-matched targets in the 3′ UTR were the most robustly suppressed upon miR-320a transfection (Figs 3E and S7B). The notable exception was *ADAM19*, which was only slightly repressed. Given the abundance of non-canonical sites in our study and many others, they likely represent different paradigms for targeting and function [34–36,83,85], while non-repressed targets may represent transient binding events that do not negatively impact target protein expression [33].

Alternative cleavage by Drosha and Dicer, and modification by exonucleases and nucleotidyl transferases can produce various templated and non-templated isomiRs [86,87]. IsomiRs can exert different targeting modes, increasing the complexity of miRNA target identification. In particular, 3′ uridylation allows miRNAs to target non-canonical targets without seed matches [88]. Since qCLASH ligates miRNAs to their targets, endogenous modifications, like trimming and tailing, could be captured while miRNAs are base-paired with a specific set of targets. The use of qCLASH allows genome-wide identification of such events that would otherwise be passed over with bioinformatic predictions or AGO-CLIP. Additionally, qCLASH

can be used to identify novel miRNA with TOMiD (target oriented miRNA discovery), a database-naïve bioinformatic method for identifying miRNA in chimeric reads [49]. In TOMiD, reads that do not fully align to a single reference sequence are parsed for characteristics of miRNA hybrids. Thus, hybrids for miRNA reads can be identified without reference sequences for miRNAs, allowing a non-biased search for novel miRNAs. Here we presented the traditional utility of qCLASH to identify TSS-miRNA targets.

miR-320a stimulates the unfolded protein response

TSS-miRNAs are generated in an evolutionarily conserved mechanism that indicates the importance of their expression [20,21]. However, the targets and the roles of TSS-miRNAs remain poorly understood, especially in the context of cancer. Mutations in miRNA processing genes change the miRNA interactome in Wilms tumor, melanoma, and breast cancer [24–26,28]. Furthermore, in breast cancer and Wilms tumor, *DROSHA* down-regulation was coupled with increased expression of Drosha-independent miRNAs [24,30]. Identifying TSS-miRNAs' targets will be important in understanding the role this class of miRNA has in cancer where *DROSHA* is down-regulated and will facilitate the development of targeted therapies.

Using qCLASH, we were able to identify the targets of miR-320a, the most conserved and abundant TSS-miRNA in HCT116 colon cancer cells [19,38]. qCLASH successfully identified the endogenous HCT116 miRNA targetome, including targets predicted by TargetScan [33]. miR-320a is the most abundant TSS-miRNA in WT and *DROSHA* KO cells (Fig 2C and S3 Table). The pathway analysis of qCLASH-identified targets revealed that miR-320a regulates the eIF2 signaling pathway (Fig 3A). Among the high-confidence targets, the ER chaperone CANX is involved in the unfolded protein response, one arm of which involves increased eIF2 signaling to transiently suppress global protein synthesis. We identified two miR-320a binding sites in the *CANX* 3′ UTR using qCLASH (Fig 4D). Exogenously expressed miR-320a or inhibited endogenous miR-320a affects *CANX* mRNA and protein levels (Figs 3E, 4A, 4B and 4C). Mutating either binding site alone did not abate CANX reporter repression, a decrease was observed only when both were simultaneously mutated (Fig 4D and 4E). We further demonstrated that the expression of miR-320a causes constitutive activation of the UPR, in line with a previous report (Fig 5A) [58]. Finally, we found that miR-320a is down-regulated in colorectal cancers compared to normal adjacent tissue in TCGA data (S8A Fig). In mRNA and miRNA sequencing data from the same patient-derived tumor, miR-320a was down-regulated (S8B Fig), while *CANX* expression increased (S8C Fig).

The expression of miR-320a is frequently down-regulated in colorectal cancer cells. [65,66,74], and conversely, the overexpression of miR-320a reduced migration, invasion, and proliferation of tumor cells [66,72,73]. During oncogenesis, the progressive loss of miR-320a expression is associated with tumor progression [67]. Low miR-320a expression in colorectal cancer has been linked to increased incidences of metastases, the leading cause of mortality in cancer [67,89]. Loss of miR-320a is predictive of outcomes in colorectal cancer patients, with low expression being correlated with decreased survival [68]. Following the excision of tumors, miR-320a's concentration in plasma increased in patients who had clinical improvement [74]. These results strongly support using miR-320a as a biomarker for disease progression and clinal outcome. It was previously reported that miR-320a targets β-catenin, the transcriptional factor for Wnt signaling [72,90]. Frequently up-regulated, Wnt signaling is regarded as one of the main molecular drivers of oncogenesis in colorectal cancer [91]. Understanding how the loss of miR-320a expression in colorectal cancer drives oncogenesis will be important in developing targeted therapies.

Our results demonstrate how qCLASH can identify cellular pathways targeted by miRNAs in cancer cells. Specifically, we identified *CANX*, which can trigger the UPR, as a miR-320a

down-regulated target. A decline in CANX function can cause the accumulation of unfolded proteins, which leads to activation of the resident ER kinase PERK. The subsequent phosphorylation of the translation initiation factor eIF2 results in general translational suppression, but a paradoxical increase translation of ATF4, one of the main transcriptional effectors for eIF2 signaling. We demonstrated that miR-320a increases ATF4 abundance during unfolded protein-induced ER stress. ATF4 abundance is increased in a wide variety of human cancer cell types and tumor growth can be dependent on PERK activation and ATF4 expression [92,93]. However, sustained ATF4 production often leads to induction of the pro-apoptotic gene for CHOP, which in turn would promote apoptosis and programmed tumor cell death [94]. Given that miR-320a is repressed during the progression of colorectal cancer, the UPR could be dampened, allowing the tumor cells to escape apoptosis resulting from sustained ER stress signaling. In conclusion, we have used AGO-qCLASH to dissect the TSS-miRNA targetome in HCT116 colorectal cancer cells and discovered that miR-320a targets *CANX* and stimulates the UPR.

Materials and methods

Cell culture

HCT116 cells were maintained in McCoy's 5A media (Cytiva, SH30200FS), and T98G, Hela, mouse embryonic fibroblasts and 293T cells were maintained in Dulbecco's Modified Eagle's medium (Sigma-Aldrich, D5796) at 37˚C with 5% CO_2. All media were supplemented with 10% fetal bovine serum and 1X penicillin/streptomycin (Gibco, 15070063). For experiments involving thapsigargin (Sigma, T9033), tunicamycin (Sigma, T7765) and histidinol (Sigma, H6647), media were supplemented with 1X GlutaMAX (Gibco, 35050079) and 1X MEM Non-Essential Amino Acids (Gibco, 11140050).

AGO-CLASH and qCLASH

AGO-CLASH and qCLASH were conducted on HCT116 WT, *DROSHA* KO, and *DICER* KO cells as previously described with modification from Gay et al [36]. Cells were grown on 15 cm plates until 80–90% confluent, washed twice in 1X PBS (137 mM NaCl, 2.7 mM KCl, 10 mM Na_2HPO_4, 1.8 mM KH_2PO_4), and irradiated with 254 nm UV at 0.6 J/cm^2. Cell pellets were frozen at -80˚C until lysis. Pellets were resuspended in cell lysis buffer (50 mM HEPES-KOH, pH 7.5, 150 mM KCl, 2 mM EDTA, 1 mM NaF, 0.5% NP-40, 0.5 mM DTT), lysed for 15 minutes on ice, treated with 10U for RQ1 DNase (Promega, M610A) for 5 minutes at 37˚C with shaking, and centrifuged at 21,000xg for 15 minutes at 4˚C.

Six mg of Protein G Dynabeads (Invitrogen, 10004D) were washed in PBS-T three times and conjugated with 57.6 μg AffiniPure Rabbit Anti-Mouse IgG (Jackson ImmunoResearch, 315-005-008). After washing three times in PBS-T (1X PBS, 0.02% Tween-20), beads were incubated with 4 μg 2A8 anti-AGO antibody. 156 μg of Protein L Magnetic Beads (Pierce, 88850) were washed three times in PBS-T and incubated with 15.6 μg 4F9 anti-AGO antibody. Beads were washed three times in 1X PXL (1X PBS, 0.1% SDS, 0.5% sodium deoxycholate, 0.5% NP-40) and once with lysis buffer. Approximately 3 mg of lysate were pre-cleared with 3 mg unconjugated Protein G beads or 78 μg Protein L beads to minimize non-specific binding.

The pre-cleared lysate was added to beads and incubated overnight at 4˚C with gentle agitation. Lysates were removed and the beads were washed three times in lysis buffer. Each sample was incubated in 15 ng/μL RNaseA for 12 minutes at 22˚C. Intermolecular ligation and libraries were generated as previously described (S1 Text) [36]. Libraries were separated on an 8% native polyacrylamide gel and regions between 147 and 527 bp were excised and eluted overnight in 1:1 RNA elution buffer (300mM NaOAC, 25 mM Tris-HCl pH 8.0): phenol

chloroform isoamyl alcohol (PCA). The excess adapter was removed using AMPure XP beads (Beckman, A63880) following the manufacturer's instructions. Libraries were sequenced on the Illumina HiSeq 3000 by the University of Florida Interdisciplinary Center for Biotechnology Research (ICBR) NextGen DNA Sequencing Core.

Bioinformatic analysis of qCLASH libraries

Sequencing reads from qCLASH libraries were first analyzed with Trimmomatic to remove the adapter and low-quality reads [43]. PEAR was used to combine forward and reverse reads into a single forward read [44]. PCR duplicates were removed using fastx_toolkit and the unique molecular identifier was removed by trimming the first four and last four nucleotides with Cutadapt [46,47]. Finally, reads were analyzed with Hyb to generate hyb and viennad files. A custom script was used to identify clusters between replicates for each miRNA. Individual miRNA counts from adapter-trimmed sequencing data were determined using miR-Deep2 [95]. The genome used for mapping was hg38 and miRNA sequences were obtained from miRbase v.22 [96]. Previously identified TSS-miRNAs were manually added to the miRbase file [20,21,38]. miRNA binding and miRNA seed matches were determined using custom python scripts. All scripts used in this study are available at GitHub (https://github.com/UF-Xie-Lab/qCLASH).

Quantitative reverse-transcription polymerase chain reactions (RT-qPCR) and RNA-seq

For RT-qPCR, $1x10^6$ HCT116 *DICER* KO cells were transfected with 10–20 pmols of either negative control or miR-320a mimic with 7.5 μL of Lipofectamine RNAiMAX (Invitrogen, 13778150) in a 6-well plate. After 48 hours, total RNA from cells were extracted using TRIzol (Invitrogen, 15596018). Total RNA was treated with 1U/μg RQ1 DNase at 37˚C for 30 minutes. RNA was purified by PCA and resuspended in nuclease-free water.

For RT-qPCR, DNase-treated RNA was reverse transcribed using iScript Reverse Transcription Supermix (BioRad, 1708841). The resulting cDNA was used for qPCR using the SsoAdvanced Universal SYBR Green Supermix (BioRad, 1725275). Each reaction was performed in technical and biological triplicate using 12.5 ng of cDNA. The cycling conditions used were initial denaturation at 95˚C for 30 seconds, and 40 cycles of 95˚C for 15 seconds and 60˚C for 30 seconds. Fold changes were determined using the comparative Ct method [97]. Primers used for RT-qPCR are listed in S1 Table.

For RNA-seq of mimic and antagomir transfected cells, polyA-RNAs were enriched from total RNA and sequenced by UF ICBR and Novogene. At UF ICBR, libraries were made using the NEBNext Ultra II Directional RNA Library Prep Kit following the polyA workflow (NEB, E7760). A custom protocol was used at Novogene for libraries preparation. Sequencing reads from poly-A selected RNA-seq were processed with Cutadapt to remove the residual adapter and filter for short reads using the parameter "-m 17" [47]. Trimmed pair-end reads were aligned to the human genome (Gencode—GRCh38.013) using HISAT2 with the parameters "—dta" [98]. Samtools was used to convert the output of HISAT2 into a sorted bam file [99]. Reads were assembled using StringTie and a reference transcriptome (Gencode–v37 primary Assembly) with the parameters "-e -B" [100]. Differential gene expression for assembled transcripts was determined using Ballgown as previously described [101]. Counts for genes were generated from the StringTie output using the supplied script prepDE.py3. DEseq2 was used to generate normalized counts [102].

For gene expression of *DICER* KO cells, total RNA was extracted and polyA selected libraries were prepared by Novogene. Data analysis was conducted by the UF ICBR Bioinformatics

Core. Briefly, Trimmomatic was used to remove adapter sequences and poor quality reads [43]. Reads were aligned to the genome (GRCh38 - https://useast.ensembl.org/Homo_sapiens/Info/Index/) using STAR [103]. Gene expression was determined by extracting the FPKM from aligned reads using RSEM [104].

Pathway analysis

Ingenuity Pathway Analysis (IPA) (Qiagen) was used to identify pathways targeted by miR-320a. We identified 815 miR-320a targets that appear in two out of five replicates from WT cells and 327 targets that appear in two out of four replicates from *DROSHA* KO cells. Each set was run through IPA's core analysis to identify significantly targeted pathways. For RNA-seq experiments, differentially expressed genes ($p \leq 0.05$) were analyzed using IPA's core analysis.

Antibodies and Western blot

HCT116 and 293T cells were sonicated in RIPA lysis buffer (50 nM Tris-HCL pH 8.0, 1% Triton X-100, 0.5% sodium deoxycholate, 0.1% SDS, 150 nM sodium chloride, 2 mM EDTA pH 8.0, 1X cOmplete EDTA-free (Roche, 05056489001)) until cleared. Protein concentration was determined using the DC Protein Assay Kit II (BioRad, 5000112) following the manufacturer's instructions. Lysates were separated with sodium dodecyl sulfate polyacrylamide gel electrophoresis (SDS-PAGE 8–10%) and transferred to 0.2 μm nitrocellulose for western blot. Primary antibodies were -AGO2 antibody 11A9, GAPDH (1:5000–1:10000; Cell Signaling, 14C10), ATF4 (1:5000; Cocalico Biotechnology Inc.), and CANX (1:1000; Cusabio, CSB-PA00899A0Rb) and secondary antibodies were goat anti-rat IgG, HRP conjugated (Pierce, 31470) and goat anti-rabbit IgG, HRP conjugated (Pierce, 31460).

Northern blot

Northern blots were performed as previously described with either near infrared probe or ^{32}P probe [21,54,55,105]. Probes are listed in S1 Table. Total RNA was separated on 15% Urea-PAGE and transferred to nylon membrane. UV crosslinking and Hybond N+ membrane was used for HCT116 WT and HCT116 *DICER* KO total RNA. EDC crosslinking and Hybond NX membrane was used for HCT116 *DROSHA* KO total RNA.

Integrated stress response induction

Cells were seeded in 6-well and 12-well plates at a density of $1.25x10^5$-$5x10^5$ cells per well and transfected with miR-320a mimic (Qiagen, 339173 YM00471432) or antagomir (GenePharma) 18–24 hours after seeding with Lipofectamine RNAiMax. A plasmid containing endogenous miR-320a gene was transfected with polyethylenimine (PEI) (Polysciences Inc, 24765–1) [19]. The medium was replenished 12 hours after transfection. 50 nM thapsigargin, 2 μg/mL tunicamycin, or 2 mM histidinol was added 24 hours after transfection and incubated for the designated time before being collected for western blot.

Luciferase assays

Regions corresponding to the qCLASH-identified miRNA binding site along with flanking regions were PCR amplified using Phusion High-Fidelity DNA Polymerase. CANX fragments were cloned into pmirGlo (Promega, E1330) using In-Fusion HD Cloning Kit (Takara, 639649). Mutants for miR-320a sites were generated using site-directed mutagenesis by replacing the miR-320a seed match sequence with the HVS miR-HSUR4 seed match sequence. For luciferase assays, $2.5x10^5$ 293T cells per well were plated in a 12-well plate. After 18–24 hours

of incubation, cells were transfected with 500 ng of reporter and miRNA-vector using 4 μg PEI. Dual-luciferase assays were carried out using the Dual-Luciferase Reporter Assay System (Promega, E19080). After 48 hours, cells were lysed with 1X passive lysis buffer for 15 minutes at room temperature with shaking. Firefly luciferase activity was measured by adding 25 μL Luciferase Assay Buffer II (LARII) to 5 μL of lysate and measured immediately with the Glo-Max 20/20 Luminometer (Promega, E5311). Reactions were stopped and Renilla luciferase activity was measured by adding 25 μL Stop&Go reagent. Samples were measured in technical and biological triplicate.

miR-320a expression in The Cancer Genome Atlas

Normalized expression of miR-320a in cancerous tissues and adjacent normal tissues from the TCGA Research Network (https://www.cancer.gov/tcga) was acquired from UCSC Xena (https://xenabrowser.net/) [62,63].

Supporting information

S1 Text. Supplemental Materials and Methods.
(PDF)

S1 Fig. AGO-CLASH library preparation. (A) AGO immunoprecipitation with 2A8 and 4F9 AGO antibodies in HCT116 cells. Cells were lysed and incubated with antibody-bound beads. I (input) and S (supernatant) are 1/15 of P (pellet). (B) RNA enriched by AGO-IP was labeled with ^{32}P using T4 PNK, separated on SDS-PAGE, and transferred to nitrocellulose. The boxes mark where the membrane was excised for CLASH library prep. AGO2 was detected by Western blot with the 11A9 antibody. (C) 2% of each cDNA library was PCR amplified with 10, 12, and 14 cycles to determine the optimal number of cycles (3 less than when the smear begins to appear). The boxes indicate the expected library range.
(EPS)

S2 Fig. miRNA-CLASH methodology isolated similar target genes as AGO-CLASH. (A) Schematic depicting the principle of a miR-specific primer to generate a single miRNA qCLASH library. The RP1 primer has the miR-320a sequence (minus 2 nucleotides) added to the 3′ end. (B) Venn diagram depicting the overlap of miR-320a target genes in qCLASH and miR-qCLASH.
(EPS)

S3 Fig. Qualitative analysis of qCLASH. (A) *DROSHA* KO results in a global reduction of canonical miRNAs. The expression of each miRNA was normalized to miR320a in *DROSHA* KO cells compared to WT cells. TSS-miRNAs are labeled in magenta, mirtron miR-877 labeled in green, miR-snaR labeled in purple. (B) Drosha-independent miRNAs are ranked high in *DROSHA* KO cells. The expression of miRNAs was determined using miR-Deep2 and averaged together. The top 200 miRNAs expressed in WT cells were compared to their ranking in *DROSHA* KO cells. (C) No correlation was found between the number of miR-320a hybrids identified for each gene in qCLASH and the expression of the gene (RPKM) in *DICER* KO cells. The correlation coefficient (r) is depicted on the graph.
(EPS)

S4 Fig. miR-320a is involved in the eIF2 signaling pathway. (A) miR-320a targets from WT qCLASH are enriched in the eIF2 pathway. Purple outlines denote that miR-320a target genes in a component or process are enriched, and grey shapes denote a direct target of miR-320a as determined by qCLASH. (B) Differentially expressed genes in miR-320a transfected *DICER*

KO cells are enriched in the eIF2 pathway. Purple outlines indicate differentially expressed genes in a component or process are enriched, green denotes down-regulation, red denotes up-regulation, grey shapes are not significant ($p > 0.05$).
(EPS)

S5 Fig. miR-320a mimic and antagomir transfection in HCT116 WT, *DROSHA* KO, and *DICER* KO cells. (A) GFP reporter containing two complementary miR-320a binding sites in the 3′ UTR was expressed in WT, *DROSHA* KO, and *DICER* KO. *Top right*–WT cells were co-transfected with miR-320a and GFP reporter. *Bottom left*–*DROSHA* KO and *Bottom right*–*DICER* KO cells stably expressing GFP reporter were transfected with miR-320a antagomir and mimic, respectively. miR-320a mimic suppressed the GFP reporter in *DICER* KO and WT cells. Antagomir suppresses miR-320a levels signified by increased GFP expression in *DROSHA* KO cells. Images were taken 48 hours after transfection. (B) irNorthern blot of miR-320a and U6 in total RNA extracted from WT, *DROSHA* KO, and *DICER* KO cells treated with miR-320a mimic or antagomir. (C) Cumulative distribution of mRNA fold changes in miR-320a antagomir-transfected HCT116 *DROSHA* KO cells; Blue line: conserved miR-320a targets from TargetScan; Red line: qCLASH-identified miR-320a targets appeared in at least three replicates in WT cells; Black line: all transcripts. P-values were determined using Kolmogorov Smirnov tests between colored subsets and the control.
(EPS)

S6 Fig. Ingenuity Pathway Analysis (IPA) reveals that miR-320a targets eIF2 signaling. (A) WT cells were transfected with miR-320a mimic. Differentially expressed genes determined by polyA RNA-seq ($p \leq 0.05$) were analyzed with IPA, where eIF2 signaling is in the top 10 enriched pathways. (B) *DROSHA* KO cells were transfected with miR-320a antagomir. Differentially expressed genes determined by polyA RNA-seq ($p \leq 0.05$) were analyzed with IPA, revealing eIF2 signaling as significantly enriched. The dotted line represents IPA's cutoff for significantly expressed genes ($-\log_2$ p-value ≥ 1.3).
(EPS)

S7 Fig. Predicted base-pairing interactions in high confidence miR-320a hybrids identified in qCLASH. High confidence targets with canonical seed matches (A) and non-canonical seed matches (B) are depicted. The microRNA seed region is marked as magenta. The target site's location in the transcript is denoted.
(EPS)

S8 Fig. miR-320a and *CANX* are negatively correlated in colorectal cancer. (A) The Cancer Genome Atlas (TCGA) gene expression of miR-320a in cancer cells compared to surrounding healthy tissue. Significant changes ($p \leq 0.05$) between Normal (N) and Tumor (T) are marked in red. Patient-derived miRNA and mRNA sequencing data of (B) miR-320a and (C) *CANX* expression in tumor (CRC) compared to adjacent non-tumor cells (ctrl). Significant differences were measured with paired T-test. ns = $P > 0.05$, * = $P \leq 0.05$. Bladder urothelial carcinoma (BLCA), Breast invasive carcinoma (BRCA), Cervical squamous cell carcinoma and endocervical adenocarcinoma (CESC), Cholangiocarcinoma (CHOL), Colon adenocarcinoma (COAD), Esophageal carcinoma (ESCA), Head and Neck squamous cell carcinoma (HNSC), Kidney Chromophobe (KICH), Kidney renal clear cell carcinoma (KIRC), Kidney renal papillary cell carcinoma (KIRP), Liver hepatocellular carcinoma (LIHC), Lung adenocarcinoma (LUAD), Lung squamous cell carcinoma (LUSC), Pancreatic adenocarcinoma (PAAD), Pheochromocytoma and Paraganglioma (PCPG), Prostate adenocarcinoma (PRAD), Rectum adenocarcinoma (READ), Skin Cutaneous Melanoma (SKCM), Stomach adenocarcinoma (STAD), Thyroid carcinoma (THCA), Thymoma (THYM), Uterine Corpus Endometrial

Carcinoma (UCEC).
(EPS)

S9 Fig. miR-320a affects UPR/ISR. Western blot of ATF4, CANX and GAPDH in miR-320a mimic-transfected (A) HCT116 cells and (B) 293T cells treated with thapsigargin (Tg) for various times. irNorthern for miR-320a in HCT116 and 293T cells treated with (C) Tg and (D) tunicamycin (Tm). * marks a non-specific band detected by miR-320a probe in 293T cells.
(TIF)

S10 Fig. miR-320a affects UPR in different cell lines. (A) Representative western blot of ATF4 in miR-320a expression plasmid-transfected HEK293T cells treated with Tg or Tm. Representative western blot of ATF4 in miR-320a mimic-transfected T98G (B), HeLa (C) cells and antagomir-transfected DAOY cells (D) with Tg treatment. GAPDH serves as a loading control. Relative ATF4 levels after miR-320a mimic or antagomir transfection is indicated below the blot.
(EPS)

S1 Table. List of oligonucleotides used in this study.
(XLSX)

S2 Table. Summary of CLASH, qCLASH, and miR-qCLASH. Summary of CLASH, qCLASH, and miR-320a-qCLASH data. "AB" depicts which AGO antibody was used for IP. "Region" refers to the area on the membrane that was excised for CLASH. Percentage depicts the fraction of miRNA hybrids of the specific miRNA in total miRNA/mRNA hybrids. BR = Biological replicate.
(XLSX)

S3 Table. Summary of qCLASH. Table summary of biological replicates of qCLASH. "AB" depicts which AGO antibody was used for IP. Percentage depicts the fraction of hybrids of the specific miRNA in total miRNA/mRNA hybrids. BR = Biological replicate.
(XLSX)

S4 Table. AGO-qCLASH identified miR-320a targets in WT cells. Table of miR-320a targets in WT cells identified in at least two biological replicates. Replicate refers to the number of different samples each hybrid is identified in. Peak refers to the total number of reads from all replicates.
(XLSX)

S5 Table. AGO-qCLASH identified miR-320a targets in *DROSHA* KO cells. Table of miR-320a targets in *DROSHA* KO cells identified in at least two biological replicates. Replicate refers to the number of biological samples each hybrid is identified in. Peak refers to the total number of reads from all replicates.
(XLSX)

Acknowledgments

We thank Drs. Edward Chan, William Dunn, Narry Kim, Michael Kladde, Grzegorz Kudla, and Zissimos Mourelatos for sharing reagents and protocols; Tracy Ouncap for proofreading; UF Interdisciplinary Center for Biotechnology Research for services in high-throughput DNA Sequencing, and AGO 4F9 antibody production; UF Health Cancer Center Biostatistics & Quantitative Sciences Shared Resources for access to Ingenuity Pathway Analysis and the UF Health Cancer Center Cancer Informatics Shared Resource.

Author Contributions

Conceptualization: Christopher J. Fields, Michael S. Kilberg, Mingyi Xie.

Data curation: Christopher J. Fields, Lu Li, Nicholas M. Hiers, Tianqi Li, Peike Sheng, Taha Huda.

Formal analysis: Christopher J. Fields, Lu Li, Nicholas M. Hiers, Tianqi Li, Peike Sheng.

Funding acquisition: Jiang Bian, Michael S. Kilberg, Rolf Renne, Mingyi Xie.

Investigation: Christopher J. Fields, Nicholas M. Hiers, Tianqi Li, Peike Sheng, Taha Huda.

Methodology: Christopher J. Fields, Lu Li, Taha Huda, Jixiu Shan, Lauren Gay, Michael S. Kilberg, Rolf Renne, Mingyi Xie.

Project administration: Mingyi Xie.

Resources: Lu Li, Jixiu Shan, Lauren Gay, Tongjun Gu, Jiang Bian, Michael S. Kilberg, Rolf Renne, Mingyi Xie.

Software: Christopher J. Fields, Lu Li, Tongjun Gu.

Supervision: Mingyi Xie.

Validation: Christopher J. Fields, Nicholas M. Hiers, Tianqi Li, Peike Sheng.

Visualization: Christopher J. Fields, Mingyi Xie.

Writing – original draft: Christopher J. Fields, Mingyi Xie.

Writing – review & editing: Christopher J. Fields, Michael S. Kilberg, Mingyi Xie.

References

1. Friedman RC, Farh KK-H, Burge CB, Bartel DP. Most mammalian mRNAs are conserved targets of microRNAs. Genome Res. 2009; 19: 92–105. https://doi.org/10.1101/gr.082701.108 PMID: 18955434
2. Lee Y. MicroRNA maturation: stepwise processing and subcellular localization. The EMBO Journal. 2002; 21: 4663–4670. https://doi.org/10.1093/emboj/cdf476 PMID: 12198168
3. Lee Y, Ahn C, Han J, Choi H, Kim J, Yim J, et al. The nuclear RNase III Drosha initiates microRNA processing. Nature. 2003; 425: 415–419. https://doi.org/10.1038/nature01957 PMID: 14508493
4. Nguyen TA, Jo MH, Choi Y-G, Park J, Kwon SC, Hohng S, et al. Functional Anatomy of the Human Microprocessor. Cell. 2015; 161: 1374–1387. https://doi.org/10.1016/j.cell.2015.05.010 PMID: 26027739
5. MacRae IJ. Structural Basis for Double-Stranded RNA Processing by Dicer. Science. 2006; 311: 195–198. https://doi.org/10.1126/science.1121638 PMID: 16410517
6. Khvorova A, Reynolds A, Jayasena SD. Functional siRNAs and miRNAs Exhibit Strand Bias. Cell. 2003; 115: 209–216. https://doi.org/10.1016/s0092-8674(03)00801-8 PMID: 14567918
7. Bartel DP. Metazoan MicroRNAs. Cell. 2018; 173: 20–51. https://doi.org/10.1016/j.cell.2018.03.006 PMID: 29570994
8. Behm-Ansmant I, Rehwinkel J, Doerks T, Stark A, Bork P, Izaurralde E. mRNA degradation by miRNAs and GW182 requires both CCR4:NOT deadenylase and DCP1:DCP2 decapping complexes. Genes Dev. 2006; 20: 1885–1898. https://doi.org/10.1101/gad.1424106 PMID: 16815998
9. Xie M, Steitz JA. Versatile microRNA biogenesis in animals and their viruses. RNA Biology. 2014; 11: 673–681. https://doi.org/10.4161/rna.28985 PMID: 24823351
10. Ha M, Kim VN. Regulation of microRNA biogenesis. Nat Rev Mol Cell Biol. 2014; 15: 509–524. https://doi.org/10.1038/nrm3838 PMID: 25027649
11. Yang J-S, Maurin T, Robine N, Rasmussen KD, Jeffrey KL, Chandwani R, et al. Conserved vertebrate mir-451 provides a platform for Dicer-independent, Ago2-mediated microRNA biogenesis. Proc Natl Acad Sci U S A. 2010; 107: 15163–15168. https://doi.org/10.1073/pnas.1006432107 PMID: 20699384

12. Cheloufi S, Dos Santos CO, Chong MMW, Hannon GJ. A dicer-independent miRNA biogenesis pathway that requires Ago catalysis. Nature. 2010; 465: 584–589. https://doi.org/10.1038/nature09092 PMID: 20424607

13. Cifuentes D, Xue H, Taylor DW, Patnode H, Mishima Y, Cheloufi S, et al. A Novel miRNA Processing Pathway Independent of Dicer Requires Argonaute2 Catalytic Activity. Science. 2010; 328: 1694–1698. https://doi.org/10.1126/science.1190809 PMID: 20448148

14. Kretov DA, Walawalkar IA, Mora-Martin A, Shafik AM, Moxon S, Cifuentes D. Ago2-Dependent Processing Allows miR-451 to Evade the Global MicroRNA Turnover Elicited during Erythropoiesis. Molecular Cell. 2020; S1097276520301131. https://doi.org/10.1016/j.molcel.2020.02.020 PMID: 32191872

15. Zhang L, Sankaran VG, Lodish HF. MicroRNAs in erythroid and megakaryocytic differentiation and megakaryocyte–erythroid progenitor lineage commitment. Leukemia. 2012; 26: 2310–2316. https://doi.org/10.1038/leu.2012.137 PMID: 22617791

16. Okamura K, Hagen JW, Duan H, Tyler DM, Lai EC. The Mirtron Pathway Generates microRNA-Class Regulatory RNAs in Drosophila. Cell. 2007; 130: 89–100. https://doi.org/10.1016/j.cell.2007.06.028 PMID: 17599402

17. Berezikov E, Chung W-J, Willis J, Cuppen E, Lai EC. Mammalian Mirtron Genes. Molecular Cell. 2007; 28: 328–336. https://doi.org/10.1016/j.molcel.2007.09.028 PMID: 17964270

18. Ruby JG, Jan CH, Bartel DP. Intronic microRNA precursors that bypass Drosha processing. Nature. 2007; 448: 83–86. https://doi.org/10.1038/nature05983 PMID: 17589500

19. Xie M, Li M, Vilborg A, Lee N, Shu M-D, Yartseva V, et al. Mammalian 5′-Capped MicroRNA Precursors that Generate a Single MicroRNA. Cell. 2013; 155: 1568–1580. https://doi.org/10.1016/j.cell.2013.11.027 PMID: 24360278

20. Zamudio JR, Kelly TJ, Sharp PA. Argonaute-Bound Small RNAs from Promoter-Proximal RNA Polymerase II. Cell. 2014; 156: 920–934. https://doi.org/10.1016/j.cell.2014.01.041 PMID: 24581493

21. Sheng P, Fields C, Aadland K, Wei T, Kolaczkowski O, Gu T, et al. Dicer cleaves 5′-extended microRNA precursors originating from RNA polymerase II transcription start sites. Nucleic Acids Research. 2018; 46: 5737–5752. https://doi.org/10.1093/nar/gky306 PMID: 29746670

22. Cui Y, Lyu X, Ding L, Ke L, Yang D, Pirouz M, et al. Global miRNA dosage control of embryonic germ layer specification. Nature. 2021; 593: 602–606. https://doi.org/10.1038/s41586-021-03524-0 PMID: 33953397

23. Khan AA, Betel D, Miller ML, Sander C, Leslie CS, Marks DS. Transfection of small RNAs globally perturbs gene regulation by endogenous microRNAs. Nature Biotechnology. 2009; 27: 549–555. https://doi.org/10.1038/nbt.1543 PMID: 19465925

24. Dedes KJ, Natrajan R, Lambros MB, Geyer FC, Lopez-Garcia MA, Savage K, et al. Down-regulation of the miRNA master regulators Drosha and Dicer is associated with specific subgroups of breast cancer. Eur J Cancer. 2011; 47: 138–150. https://doi.org/10.1016/j.ejca.2010.08.007 PMID: 20832293

25. Torres A, Torres K, Paszkowski T, Jodłowska-Jędrych B, Radomański T, Książek A, et al. Major regulators of microRNAs biogenesis Dicer and Drosha are down-regulated in endometrial cancer. Tumour Biol. 2011; 32: 769–776. https://doi.org/10.1007/s13277-011-0179-0 PMID: 21559780

26. Jafarnejad SM, Sjoestroem C, Martinka M, Li G. Expression of the RNase III enzyme DROSHA is reduced during progression of human cutaneous melanoma. Modern Pathology. 2013; 26: 902–910. https://doi.org/10.1038/modpathol.2012.225 PMID: 23370771

27. Torrezan GT, Ferreira EN, Nakahata AM, Barros BDF, Castro MTM, Correa BR, et al. Recurrent somatic mutation in DROSHA induces microRNA profile changes in Wilms tumour. Nat Commun. 2014; 5: 4039. https://doi.org/10.1038/ncomms5039 PMID: 24909261

28. Chen KS, Stroup EK, Budhipramono A, Rakheja D, Nichols-Vinueza D, Xu L, et al. Mutations in microRNA processing genes in Wilms tumors derepress the *IGF2* regulator *PLAG1*. Genes & Development. 2018; 32: 996–1007. https://doi.org/10.1101/gad.313783.118 PMID: 30026293

29. Gadd S, Huff V, Walz AL, Ooms AHAG, Armstrong AE, Gerhard DS, et al. A Children's Oncology Group and TARGET initiative exploring the genetic landscape of Wilms tumor. Nat Genet. 2017; 49: 1487–1494. https://doi.org/10.1038/ng.3940 PMID: 28825729

30. Walz AL, Ooms A, Gadd S, Gerhard DS, Smith MA, Guidry Auvil JM, et al. Recurrent DGCR8, DROSHA, and SIX homeodomain mutations in favorable histology Wilms tumors. Cancer Cell. 2015; 27: 286–297. https://doi.org/10.1016/j.ccell.2015.01.003 PMID: 25670082

31. Chi SW, Zang JB, Mele A, Darnell RB. Argonaute HITS-CLIP decodes microRNA–mRNA interaction maps. Nature. 2009; 460: 479–486. https://doi.org/10.1038/nature08170 PMID: 19536157

32. Hafner M, Landthaler M, Burger L, Khorshid M, Hausser J, Berninger P, et al. Transcriptome-wide Identification of RNA-Binding Protein and MicroRNA Target Sites by PAR-CLIP. Cell. 2010; 141: 129–141. https://doi.org/10.1016/j.cell.2010.03.009 PMID: 20371350

33. Agarwal V, Bell GW, Nam J-W, Bartel DP. Predicting effective microRNA target sites in mammalian mRNAs. Elife. 2015;4. https://doi.org/10.7554/eLife.05005 PMID: 26267216

34. Helwak A, Kudla G, Dudnakova T, Tollervey D. Mapping the Human miRNA Interactome by CLASH Reveals Frequent Noncanonical Binding. Cell. 2013; 153: 654–665. https://doi.org/10.1016/j.cell.2013.03.043 PMID: 23622248

35. Moore MJ, Scheel TKH, Luna JM, Park CY, Fak JJ, Nishiuchi E, et al. miRNA–target chimeras reveal miRNA 3′-end pairing as a major determinant of Argonaute target specificity. Nature Communications. 2015;6. https://doi.org/10.1038/ncomms9864 PMID: 26602609

36. Gay LA, Sethuraman S, Thomas M, Turner PC, Renne R. Modified Cross-Linking, Ligation, and Sequencing of Hybrids (qCLASH) Identifies Kaposi's Sarcoma-Associated Herpesvirus MicroRNA Targets in Endothelial Cells. Longnecker RM, editor. Journal of Virology. 2018; 92: e02138–17. https://doi.org/10.1128/JVI.02138-17 PMID: 29386283

37. Bullard WL, Kara M, Gay LA, Sethuraman S, Wang Y, Nirmalan S, et al. Identification of murine gammaherpesvirus 68 miRNA-mRNA hybrids reveals miRNA target conservation among gammaherpesviruses including host translation and protein modification machinery. Feng P, editor. PLoS Pathog. 2019; 15: e1007843. https://doi.org/10.1371/journal.ppat.1007843 PMID: 31393953

38. Kim Y-K, Kim B, Kim VN. Re-evaluation of the roles of *DROSHA*, *Exportin 5*, and *DICER* in microRNA biogenesis. Proceedings of the National Academy of Sciences. 2016; 113: E1881–E1889. https://doi.org/10.1073/pnas.1602532113 PMID: 26976605

39. Nelson PT, De Planell-Saguer M, Lamprinaki S, Kiriakidou M, Zhang P, O'Doherty U, et al. A novel monoclonal antibody against human Argonaute proteins reveals unexpected characteristics of miRNAs in human blood cells. RNA. 2007; 13: 1787–1792. https://doi.org/10.1261/rna.646007 PMID: 17720879

40. Haecker I, Gay LA, Yang Y, Hu J, Morse AM, McIntyre LM, et al. Ago HITS-CLIP Expands Understanding of Kaposi's Sarcoma-associated Herpesvirus miRNA Function in Primary Effusion Lymphomas. Damania B, editor. PLoS Pathogens. 2012; 8: e1002884. https://doi.org/10.1371/journal.ppat.1002884 PMID: 22927820

41. Moore MJ, Zhang C, Gantman EC, Mele A, Darnell JC, Darnell RB. Mapping Argonaute and conventional RNA-binding protein interactions with RNA at single-nucleotide resolution using HITS-CLIP and CIMS analysis. Nature Protocols. 2014; 9: 263–293. https://doi.org/10.1038/nprot.2014.012 PMID: 24407355

42. Ikeda K, Satoh M, Pauley KM, Fritzler MJ, Reeves WH, Chan EKL. Detection of the argonaute protein Ago2 and microRNAs in the RNA induced silencing complex (RISC) using a monoclonal antibody. Journal of Immunological Methods. 2006; 317: 38–44. https://doi.org/10.1016/j.jim.2006.09.010 PMID: 17054975

43. Bolger AM, Lohse M, Usadel B. Trimmomatic: a flexible trimmer for Illumina sequence data. Bioinformatics. 2014; 30: 2114–2120. https://doi.org/10.1093/bioinformatics/btu170 PMID: 24695404

44. Zhang J, Kobert K, Flouri T, Stamatakis A. PEAR: a fast and accurate Illumina Paired-End reAd mergeR. Bioinformatics. 2014; 30: 614–620. https://doi.org/10.1093/bioinformatics/btt593 PMID: 24142950

45. Kim H, Kim J, Kim K, Chang H, You K, Kim VN. Bias-minimized quantification of microRNA reveals widespread alternative processing and 3′ end modification. Nucleic Acids Research. 2019; 47: 2630–2640. https://doi.org/10.1093/nar/gky1293 PMID: 30605524

46. Hannon G. FASTX-Toolkit. 2009. Available: http://hannonlab.cshl.edu/fastx_toolkit/index.html

47. Martin M. Cutadapt removes adapter sequences from high-throughput sequencing reads. EMBnet. journal. 2011; 17: 10. https://doi.org/10.14806/ej.17.1.200

48. Travis AJ, Moody J, Helwak A, Tollervey D, Kudla G. Hyb: A bioinformatics pipeline for the analysis of CLASH (crosslinking, ligation and sequencing of hybrids) data. Methods. 2014; 65: 263–273. https://doi.org/10.1016/j.ymeth.2013.10.015 PMID: 24211736

49. Stribling D, Lei Y, Guardia CM, Li L, Fields CJ, Nowialis P, et al. A non-canonical microRNA derived from the snaR-A non-coding RNA targets a metastasis inhibitor. RNA. 2021. https://doi.org/10.1261/rna.078694.121 PMID: 33795480

50. Broughton JP, Lovci MT, Huang JL, Yeo GW, Pasquinelli AE. Pairing beyond the Seed Supports MicroRNA Targeting Specificity. Mol Cell. 2016; 64: 320–333. https://doi.org/10.1016/j.molcel.2016.09.004 PMID: 27720646

51. Wang Y, Soneson C, Malinowska AL, Laski A, Ghosh S, Kanitz A, et al. MiR-CLIP reveals iso-miR selective regulation in the miR-124 targetome. Nucleic Acids Research. 2021; 49: 25–37. https://doi.org/10.1093/nar/gkaa1117 PMID: 33300035

52. Imig J, Brunschweiger A, Brümmer A, Guennewig B, Mittal N, Kishore S, et al. miR-CLIP capture of a miRNA targetome uncovers a lincRNA H19–miR-106a interaction. Nat Chem Biol. 2015; 11: 107–114. https://doi.org/10.1038/nchembio.1713 PMID: 25531890

53. Jin HY, Gonzalez-Martin A, Miletic AV, Lai M, Knight S, Sabouri-Ghomi M, et al. Transfection of microRNA Mimics Should Be Used with Caution. Front Genet. 2015;6. https://doi.org/10.3389/fgene.2015.00006 PMID: 25688259

54. Miller BR, Wei T, Fields CJ, Sheng P, Xie M. Near-infrared fluorescent northern blot. RNA. 2018; 24: 1871–1877. https://doi.org/10.1261/rna.068213.118 PMID: 30201850

55. Fields C, Sheng P, Miller B, Wei T, Xie M. Northern Blot with IR Fluorescent Probes: Strategies for Probe Preparation. Bio Protoc. 2019; 9: e3219. https://doi.org/10.21769/BioProtoc.3219 PMID: 31428663

56. Ellgaard L, Frickel E-M. Calnexin, calreticulin, and ERp57: teammates in glycoprotein folding. Cell Biochem Biophys. 2003; 39: 223–247. https://doi.org/10.1385/CBB:39:3:223 PMID: 14716078

57. Uvarov AV, Mesaeli N. Enhanced ubiquitin-proteasome activity in calreticulin deficient cells: a compensatory mechanism for cell survival. Biochim Biophys Acta. 2008; 1783: 1237–1247. https://doi.org/10.1016/j.bbamcr.2008.03.004 PMID: 18405668

58. Coe H, Bedard K, Groenendyk J, Jung J, Michalak M. Endoplasmic reticulum stress in the absence of calnexin. Cell Stress Chaperones. 2008; 13: 497–507. https://doi.org/10.1007/s12192-008-0049-x PMID: 18528784

59. Hetz C, Zhang K, Kaufman RJ. Mechanisms, regulation and functions of the unfolded protein response. Nat Rev Mol Cell Biol. 2020; 21: 421–438. https://doi.org/10.1038/s41580-020-0250-z PMID: 32457508

60. Ron D, Walter P. Signal integration in the endoplasmic reticulum unfolded protein response. Nat Rev Mol Cell Biol. 2007; 8: 519–529. https://doi.org/10.1038/nrm2199 PMID: 17565364

61. Walter P, Ron D. The Unfolded Protein Response: From Stress Pathway to Homeostatic Regulation. Science. 2011; 334: 1081–1086. https://doi.org/10.1126/science.1209038 PMID: 22116877

62. Goldman MJ, Craft B, Hastie M, Repečka K, McDade F, Kamath A, et al. Visualizing and interpreting cancer genomics data via the Xena platform. Nat Biotechnol. 2020; 38: 675–678. https://doi.org/10.1038/s41587-020-0546-8 PMID: 32444850

63. The Cancer Genome Atlas Research Network, Weinstein JN, Collisson EA, Mills GB, Shaw KRM, Ozenberger BA, et al. The Cancer Genome Atlas Pan-Cancer analysis project. Nat Genet. 2013; 45: 1113–1120. https://doi.org/10.1038/ng.2764 PMID: 24071849

64. Tadano T, Kakuta Y, Hamada S, Shimodaira Y, Kuroha M, Kawakami Y, et al. MicroRNA-320 family is downregulated in colorectal adenoma and affects tumor proliferation by targeting CDK6. WJGO. 2016; 8: 532. https://doi.org/10.4251/wjgo.v8.i7.532 PMID: 27559432

65. Hu J, Yue X, Liu J, Kong D. Construction of an miRNA-gene regulatory network in colorectal cancer through integrated analysis of mRNA and miRNA microarrays. Mol Med Rep. 2018; 18: 5109–5116. https://doi.org/10.3892/mmr.2018.9505 PMID: 30272280

66. Zhao H, Dong T, Zhou H, Wang L, Huang A, Feng B, et al. miR-320a suppresses colorectal cancer progression by targeting Rac1. Carcinogenesis. 2014; 35: 886–895. https://doi.org/10.1093/carcin/bgt378 PMID: 24265291

67. Zhang Y, He X, Liu Y, Ye Y, Zhang H, He P, et al. microRNA-320a inhibits tumor invasion by targeting neuropilin 1 and is associated with liver metastasis in colorectal cancer. Oncol Rep. 2012; 27: 685–694. https://doi.org/10.3892/or.2011.1561 PMID: 22134529

68. Schepeler T, Reinert JT, Ostenfeld MS, Christensen LL, Silahtaroglu AN, Dyrskjøt L, et al. Diagnostic and Prognostic MicroRNAs in Stage II Colon Cancer. Cancer Res. 2008; 68: 6416–6424. https://doi.org/10.1158/0008-5472.CAN-07-6110 PMID: 18676867

69. Ryan D, Carberry S, Murphy ÁC, Lindner AU, Fay J, Hector S, et al. Calnexin, an ER-induced protein, is a prognostic marker and potential therapeutic target in colorectal cancer. J Transl Med. 2016; 14: 196. https://doi.org/10.1186/s12967-016-0948-z PMID: 27369741

70. Ge J, Jin Y, Lv X, Liao Q, Luo C, Ye G, et al. Expression profiles of circular RNAs in human colorectal cancer based on RNA deep sequencing. J Clin Lab Anal. 2019; 33: e22952. https://doi.org/10.1002/jcla.22952 PMID: 31169949

71. Röhr C, Kerick M, Fischer A, Kühn A, Kashofer K, Timmermann B, et al. High-Throughput miRNA and mRNA Sequencing of Paired Colorectal Normal, Tumor and Metastasis Tissues and Bioinformatic

Modeling of miRNA-1 Therapeutic Applications. Csermely P, editor. PLoS ONE. 2013; 8: e67461. https://doi.org/10.1371/journal.pone.0067461 PMID: 23874421

72. Sun J-Y, Huang Y, Li J-P, Zhang X, Wang L, Meng Y-L, et al. MicroRNA-320a suppresses human colon cancer cell proliferation by directly targeting β-catenin. Biochemical and Biophysical Research Communications. 2012; 420: 787–792. https://doi.org/10.1016/j.bbrc.2012.03.075 PMID: 22459450

73. Wan L-Y, Deng J, Xiang X-J, Zhang L, Yu F, Chen J, et al. miR-320 enhances the sensitivity of human colon cancer cells to chemoradiotherapy in vitro by targeting FOXM1. Biochemical and Biophysical Research Communications. 2015; 457: 125–132. https://doi.org/10.1016/j.bbrc.2014.11.039 PMID: 25446103

74. Fang Z, Tang J, Bai Y, Lin H, You H, Jin H, et al. Plasma levels of microRNA-24, microRNA-320a, and microRNA-423-5p are potential biomarkers for colorectal carcinoma. J Exp Clin Cancer Res. 2015; 34: 86. https://doi.org/10.1186/s13046-015-0198-6 PMID: 26297223

75. van Schadewijk A, van't Wout EFA, Stolk J, Hiemstra PS. A quantitative method for detection of spliced X-box binding protein-1 (XBP1) mRNA as a measure of endoplasmic reticulum (ER) stress. Cell Stress and Chaperones. 2012; 17: 275–279. https://doi.org/10.1007/s12192-011-0306-2 PMID: 22038282

76. Pakos-Zebrucka K, Koryga I, Mnich K, Ljujic M, Samali A, Gorman AM. The integrated stress response. EMBO Rep. 2016; 17: 1374–1395. https://doi.org/10.15252/embr.201642195 PMID: 27629041

77. Yoshida H, Matsui T, Yamamoto A, Okada T, Mori K. XBP1 mRNA is induced by ATF6 and spliced by IRE1 in response to ER stress to produce a highly active transcription factor. Cell. 2001; 107: 881–891. https://doi.org/10.1016/s0092-8674(01)00611-0 PMID: 11779464

78. Huang J, Pan H, Wang J, Wang T, Huo X, Ma Y, et al. Unfolded protein response in colorectal cancer. Cell Biosci. 2021; 11: 26. https://doi.org/10.1186/s13578-021-00538-z PMID: 33514437

79. Kaufman RJ. Stress signaling from the lumen of the endoplasmic reticulum: coordination of gene transcriptional and translational controls. Genes Dev. 1999; 13: 1211–1233. https://doi.org/10.1101/gad.13.10.1211 PMID: 10346810

80. Hansen BS, Vaughan MH, Wang L. Reversible inhibition by histidinol of protein synthesis in human cells at the activation of histidine. J Biol Chem. 1972; 247: 3854–3857. PMID: 4338230

81. Jiang H-Y, Wek SA, McGrath BC, Scheuner D, Kaufman RJ, Cavener DR, et al. Phosphorylation of the alpha subunit of eukaryotic initiation factor 2 is required for activation of NF-kappaB in response to diverse cellular stresses. Mol Cell Biol. 2003; 23: 5651–5663. https://doi.org/10.1128/MCB.23.16.5651-5663.2003 PMID: 12897138

82. Kozar I, Philippidou D, Margue C, Gay LA, Renne R, Kreis S. Cross-Linking Ligation and Sequencing of Hybrids (qCLASH) Reveals an Unpredicted miRNA Targetome in Melanoma Cells. Cancers. 2021; 13: 1096. https://doi.org/10.3390/cancers13051096 PMID: 33806450

83. Zhang K, Zhang X, Cai Z, Zhou J, Cao R, Zhao Y, et al. A novel class of microRNA-recognition elements that function only within open reading frames. Nat Struct Mol Biol. 2018; 25: 1019–1027. https://doi.org/10.1038/s41594-018-0136-3 PMID: 30297778

84. Chipman LB, Pasquinelli AE. miRNA Targeting: Growing beyond the Seed. Trends in Genetics. 2019; 35: 215–222. https://doi.org/10.1016/j.tig.2018.12.005 PMID: 30638669

85. Park JH, Shin S-Y, Shin C. Non-canonical targets destabilize microRNAs in human Argonautes. Nucleic Acids Res. 2017; 45: 1569–1583. https://doi.org/10.1093/nar/gkx029 PMID: 28119422

86. Neilsen CT, Goodall GJ, Bracken CP. IsomiRs—the overlooked repertoire in the dynamic microRNAome. Trends Genet. 2012; 28: 544–549. https://doi.org/10.1016/j.tig.2012.07.005 PMID: 22883467

87. van der Kwast RVCT, Quax PHA, Nossent AY. An Emerging Role for isomiRs and the microRNA Epitranscriptome in Neovascularization. Cells. 2019; 9: 61. https://doi.org/10.3390/cells9010061 PMID: 31881725

88. Yang A, Bofill-De Ros X, Shao T-J, Jiang M, Li K, Villanueva P, et al. 3′ Uridylation Confers miRNAs with Non-canonical Target Repertoires. Molecular Cell. 2019; 75: 511–522.e4. https://doi.org/10.1016/j.molcel.2019.05.014 PMID: 31178353

89. Seyfried TN, Huysentruyt LC. On the origin of cancer metastasis. Crit Rev Oncog. 2013; 18: 43–73. https://doi.org/10.1615/critrevoncog.v18.i1-2.40 PMID: 23237552

90. Bordonaro M. CREB-binding protein, p300, butyrate, and Wnt signaling in colorectal cancer. World Journal of Gastroenterology. 2015; 21: 8238. https://doi.org/10.3748/wjg.v21.i27.8238 PMID: 26217075

91. Schatoff EM, Leach BI, Dow LE. WNT Signaling and Colorectal Cancer. Curr Colorectal Cancer Rep. 2017; 13: 101–110. https://doi.org/10.1007/s11888-017-0354-9 PMID: 28413363

92. Bi M, Naczki C, Koritzinsky M, Fels D, Blais J, Hu N, et al. ER stress-regulated translation increases tolerance to extreme hypoxia and promotes tumor growth. EMBO J. 2005; 24: 3470–3481. https://doi.org/10.1038/sj.emboj.7600777 PMID: 16148948

93. Ye J, Kumanova M, Hart LS, Sloane K, Zhang H, De Panis DN, et al. The GCN2-ATF4 pathway is critical for tumour cell survival and proliferation in response to nutrient deprivation. EMBO J. 2010; 29: 2082–2096. https://doi.org/10.1038/emboj.2010.81 PMID: 20473272

94. Zinszner H, Kuroda M, Wang X, Batchvarova N, Lightfoot RT, Remotti H, et al. CHOP is implicated in programmed cell death in response to impaired function of the endoplasmic reticulum. Genes Dev. 1998; 12: 982–995. https://doi.org/10.1101/gad.12.7.982 PMID: 9531536

95. Friedländer MR, Mackowiak SD, Li N, Chen W, Rajewsky N. miRDeep2 accurately identifies known and hundreds of novel microRNA genes in seven animal clades. Nucleic Acids Research. 2012; 40: 37–52. https://doi.org/10.1093/nar/gkr688 PMID: 21911355

96. Kozomara A, Birgaoanu M, Griffiths-Jones S. miRBase: from microRNA sequences to function. Nucleic Acids Research. 2019; 47: D155–D162. https://doi.org/10.1093/nar/gky1141 PMID: 30423142

97. Schmittgen TD, Livak KJ. Analyzing real-time PCR data by the comparative CT method. Nat Protoc. 2008; 3: 1101–1108. https://doi.org/10.1038/nprot.2008.73 PMID: 18546601

98. Kim D, Paggi JM, Park C, Bennett C, Salzberg SL. Graph-based genome alignment and genotyping with HISAT2 and HISAT-genotype. Nat Biotechnol. 2019; 37: 907–915. https://doi.org/10.1038/s41587-019-0201-4 PMID: 31375807

99. Li H, Handsaker B, Wysoker A, Fennell T, Ruan J, Homer N, et al. The Sequence Alignment/Map format and SAMtools. Bioinformatics. 2009; 25: 2078–2079. https://doi.org/10.1093/bioinformatics/btp352 PMID: 19505943

100. Pertea M, Pertea GM, Antonescu CM, Chang T-C, Mendell JT, Salzberg SL. StringTie enables improved reconstruction of a transcriptome from RNA-seq reads. Nat Biotechnol. 2015; 33: 290–295. https://doi.org/10.1038/nbt.3122 PMID: 25690850

101. Pertea M, Kim D, Pertea GM, Leek JT, Salzberg SL. Transcript-level expression analysis of RNA-seq experiments with HISAT, StringTie and Ballgown. Nat Protoc. 2016; 11: 1650–1667. https://doi.org/10.1038/nprot.2016.095 PMID: 27560171

102. Love MI, Huber W, Anders S. Moderated estimation of fold change and dispersion for RNA-seq data with DESeq2. Genome Biol. 2014; 15: 550. https://doi.org/10.1186/s13059-014-0550-8 PMID: 25516281

103. Dobin A, Davis CA, Schlesinger F, Drenkow J, Zaleski C, Jha S, et al. STAR: ultrafast universal RNA-seq aligner. Bioinformatics. 2013; 29: 15–21. https://doi.org/10.1093/bioinformatics/bts635 PMID: 23104886

104. Li B, Dewey CN. RSEM: accurate transcript quantification from RNA-Seq data with or without a reference genome. BMC Bioinformatics. 2011; 12: 323. https://doi.org/10.1186/1471-2105-12-323 PMID: 21816040

105. Pall GS, Hamilton AJ. Improved northern blot method for enhanced detection of small RNA. Nat Protoc. 2008; 3: 1077–1084. https://doi.org/10.1038/nprot.2008.67 PMID: 18536652